Potent microtubule depolymerizing activity of a mitotic Kif18b-MCAK-EB network

© 2022. Published by The Company of Biologists Ltd | Journal of Cell Science (2023) 136, jcs260144. doi:10.1242/jcs.260144

RESEARCH ARTICLE

SPECIAL ISSUE: CELL BIOLOGY OF MOTORS

Potent microtubule-depolymerizing activity of a mitotic Kif18b–MCAK–EB network

Toni McHugh and Julie P. I. Welburn*

ABSTRACT

The precise regulation of microtubule length during mitosis is essential to assemble and position the mitotic spindle and segregate chromosomes. The kinesin-13 Kif2C or MCAK acts as a potent microtubule depolymerase that diffuses short distances on microtubules, whereas the kinesin-8 Kif18b is a processive motor with weak depolymerase activity. However, the individual activities of these factors cannot explain the dramatic increase in microtubule dynamics in mitosis. Using *in vitro* reconstitution and single-molecule imaging, we demonstrate that Kif18b, MCAK and the plus-end tracking protein EB3 (also known as MAPRE3) act in an integrated manner to potently promote microtubule depolymerization at very low concentrations. We find that Kif18b can transport EB3 and MCAK and promotes their accumulation to microtubule plus ends through multivalent weak interactions. Together, our work defines the mechanistic basis for a cooperative Kif18b–MCAK–EB network at microtubule plus ends, that acts to efficiently shorten and regulate microtubules in mitosis, essential for correct chromosome segregation.

KEY WORDS: Microtubule, Mitosis, Kinesin, Regulation, Depolymerization

INTRODUCTION

Within all eukaryotes, length control of microtubule polymers is essential. Microtubule length is controlled through the regulation of microtubule dynamics by motors and microtubule-associated proteins (Mitchison and Kirschner, 1984). At the onset of mitosis, the frequency of microtubule catastrophe increases dramatically, leading to disassembly of the interphase microtubule network (Belmont et al., 1990; Piehl and Cassimeris, 2003). These dynamic properties of microtubules are essential to enable the dynamic assembly and remodelling of the mitotic spindle throughout mitosis and promote chromosome alignment and segregation. In most eukaryotes, ranging from yeast to parasites and humans, the increase in catastrophe frequency is driven by the upregulation of microtubule-depolymerizing kinesin motors. These motors shorten microtubules by promoting their catastrophe (reviewed in Walczak et al., 2013). There are two major families of depolymerizing kinesins: kinesin-8 and kinesin-13. Generally, the absence of these motors is associated with defects in cell division (Gupta et al., 2006; Maney et al., 1998; Walczak et al., 1996). Yeast only have kinesin-8 motors: Kip3 and KlpB from budding yeast and *Aspergillus nidulans*, respectively, both essential for spindle positioning (Cottingham and Hoyt, 1997; Miller et al., 1998; Rischitor et al., 2004; Walczak et al., 1996). Metazoan species such as *Drosophila melanogaster* have both the kinesin-8 (Klp67) and kinesin-13 (Klp10, Klp59D) microtubule depolymerases with key roles in spindle assembly and positioning (Savoian and Glover, 2010; Goshima et al., 2005).

In mammalian cells, the kinesin-13 family consists of three members: Kif2a, Kif2b and MCAK (also known as Kif2c). Kif2a is present at centrosomes and weakly at kinetochores (Cameron et al., 2006), and Kif2b is absent from most cells and appears as a weak microtubule depolymerase in human cells (Tanenbaum et al., 2009; Welburn and Cheeseman, 2012). MCAK is the most potent and best-characterized microtubule-depolymerizing kinesin (Ems-McClung and Walczak, 2010; Friel and Welburn, 2018; Walczak et al., 2013). MCAK is strongly localized to centromeres in mitosis (Walczak et al., 1996; Wordeman et al., 1999). The endogenous localization of MCAK was reported to be cytoplasmic in interphase and at microtubule ends in mitosis (Moore et al., 2005; Tanenbaum et al., 2011; Wordeman et al., 1999). Most studies use transiently transfected MCAK tagged with a genetically encoded fluorophore to image MCAK plus-end targeting to microtubules (Moore et al., 2005). *In vitro*, rather than walking on microtubules, MCAK diffuses short distances on the microtubule lattice (Helenius et al., 2006), raising the question of how MCAK reaches the ends of crowded microtubules in the dense cytoplasm in cells. Also *in vitro*, this atypical motor associates with microtubule end-binding (EB) proteins to enhance its localization to microtubule plus ends, utilizing an SxIP-like motif, whereas in cells, disruption of this motif prevents the ability of GFP–MCAK to accumulate at microtubule ends (Honnappa et al., 2009; Montenegro Gouveia et al., 2010; Moore et al., 2005). EB3 (also known as MAPRE3)-dependent accumulation of MCAK at microtubule plus ends increases microtubule catastrophes (Montenegro Gouveia et al., 2010). However, the affinity of EB proteins for MCAK is low, around 10 µM (Buey et al., 2012).

The human kinesin-8 family has three members that regulate microtubule length: Kif19 at cilia, Kif18a on kinetochore fibres and Kif18b on astral microtubules (reviewed in Shrestha et al., 2018). The kinesin-8 motor Kif18b shortens astral microtubules in mitosis when it is released into the cytoplasm from the nucleus (Lee et al., 2010; McHugh et al., 2018; Tanenbaum et al., 2011; Walczak et al., 2016). It requires both EB proteins and its C-terminal microtubule-binding tail to accumulate at microtubule ends and depolymerize them (McHugh et al., 2018; Stout et al., 2011; Tanenbaum et al., 2011). The absence of Kif18b or MCAK leads to aberrant microtubule growth, defects in spindle assembly and positioning and lagging chromosomes (Domnitz et al., 2012; Huang et al.,

Wellcome Trust Centre for Cell Biology, School of Biological Sciences, University of Edinburgh, Edinburgh EH9 3BF, Scotland, UK.

*Author for correspondence (Julie.Welburn@ed.ac.uk)

T.M., 0000-0002-5212-3868; J.P.I.W., 0000-0002-5440-6060

Handling Editor: Michael Way
Received 21 April 2022; Accepted 21 April 2022

Journal of Cell Science (2023) 136, jcs260144. doi:10.1242/jcs.260144

2007; McHugh et al., 2018; Rankin and Wordeman, 2010). Although Kif18b shortens microtubule length through its depolymerase activity, this activity *in vitro* remains modest compared to kinesin-13 motors, and does not explain the strong depolymerization associated with Kif18b function *in vivo*. Here, using purified proteins, we show that Kif18b uses its motile properties to move MCAK and EB3 and promote their accumulation to microtubule plus ends. We also observed that MCAK and EB3 influence the motor properties of Kif18b. We reconstituted microtubule dynamics in the presence of Kif18b, EB3 and MCAK, allowing us to dissect the contributions of each factor to the activity of the network on microtubules and at microtubule plus ends. When all three components of the network were present at microtubule plus ends, we observed a large increase in catastrophe frequency, which resulted in a significant decrease in microtubule length. Overall, it is the collective effect of Kif18b, EB3 and MCAK on microtubules that enables robust change in microtubule dynamics and reduces microtubule length in mitosis.

RESULTS

Kif18b is required for microtubule plus-end localization of MCAK in cells

First, we investigated the localization of endogenous MCAK at microtubule plus ends during mitosis. In HeLa cells, we observed co-localization of MCAK with endogenous EB1 (also known as MAPRE1) that marks the plus ends of astral microtubules. We then examined the localization of MCAK in a Kif18b-knockout cell line that we had previously generated using Cas9-induced engineering, in which the long microtubule phenotype could be reversed by re-expressing Kif18b (McHugh et al., 2018). In cells lacking Kif18b (Fig. S1A), MCAK was significantly reduced at microtubule plus ends (Fig. 1A,B). These data, alongside previous work that showed microtubule plus-end reduction of MCAK after siRNA-mediated depletion of Kif18b (Tanenbaum et al., 2011), indicate that the localization of MCAK to microtubule plus ends was compromised in mitosis when Kif18b was absent both in the long and short term (Fig. 1A,B).

Kif18b localizes MCAK and EB3 to stable microtubule plus ends

Although MCAK requires Kif18b for plus-end localization, the molecular mechanism underlying this dependency is not known, despite a weak interaction reported (Tanenbaum et al., 2011). The high-resolution molecular structure of dimeric MCAK is unknown. MCAK has a complex conformation in solution that is stabilized through intramolecular interactions, which could reduce the interaction with Kif18b (Ems-McClung et al., 2013; Maney et al., 2001; McHugh et al., 2019; Zong et al., 2016). We therefore examined the Alphafold2-predicted model structure for monomeric MCAK, which revealed that a large part of the motor outside the catalytic domain is unstructured (Fig. S1B) (Jumper et al., 2021). This model correctly predicts that the final 20 residues of the C-terminus form a small helix and interact with the motor through conserved residues, which was previously shown in both *Xenopus* and human MCAK (Talapatra et al., 2015; Zong et al., 2016). We then used Colabfold, a Google Colab platform powered by AlphaFold2, to predict the structure of dimeric MCAK; however, we were not successful due to the large low-complexity regions (Mirdita et al., 2022 preprint). Similarly, much of Kif18b, apart from the catalytic domain and the dimerization domain, consists of low-complexity regions (Fig. S1C). These unstructured regions make it difficult to identify regions of interactions between MCAK and Kif18b.

To probe for the interaction between MCAK and Kif18b, we incubated Kif18b–His bound to Ni^{2+}-agarose beads with purified SNAP–$MCAK_{1–177}$ or SNAP–$MCAK_{584–725}$. We found that MCAK did not bind to Kif18b in solution (Fig. S1D,E). Thus, we hypothesized that Kif18b might interact dynamically with MCAK only in the context of the microtubules, facilitated by EB proteins that bind both Kif18b and MCAK (Honnappa et al., 2009; Montenegro Gouveia et al., 2010; Stout et al., 2011). We first tested whether Kif18b interacts with EB proteins using guanylyl-(α, β)-methylene-diphosphonate (GMPCPP)-stabilized microtubules. EB3 alone does not strongly bind to GMPCPP-stabilized microtubules (Maurer et al., 2011; Roth et al., 2018). Using *in vitro* reconstitution and total internal reflection fluorescence (TIRF) microscopy imaging, we imaged microtubules (Rhodamine, HiLyte Fluor 647), Kif18b (GFP, mRuby3), EB3 ($SNAP_{647}$–EB3) and MCAK (GFP) in the presence of 2 mM ATP. The polarity of the microtubules could be inferred because Kif18b is a microtubule plus-end-directed motor that accumulates at microtubule plus ends (McHugh et al., 2018). The amount of Kif18b accumulation at microtubule plus ends was length dependent (Fig. S2A). Recombinant $SNAP_{647}$–EB3 alone uniformly and weakly decorated the GMPCPP-stabilized microtubule lattice (Fig. 1C,D), and soluble $SNAP_{647}$–EB3 provided some background fluorescence. Upon addition of 12.5 nM Kif18b, we observed that $SNAP_{647}$–EB3 strongly colocalized with Kif18b at the plus ends of microtubules (Fig. 1C,D; Fig. S2B). Thus, on GMPCPP-stabilized microtubules, Kif18b binds EB3 and enhances the localization of EB3 to plus ends.

Based on the Kif18b-dependent localization of MCAK to microtubule plus ends in HeLa cells (Fig. 1A,B), we tested whether Kif18b influences the localization of MCAK on microtubules *in vitro*. Purified 12.5 nM MCAK–GFP bound diffusely along the length of double-stabilized (taxol and GMPCPP) microtubules (Fig. 1E,F). With the addition of 12.5 nM Kif18b–mRuby3, the localization of MCAK shifted towards the plus end of the microtubules, although MCAK still decorated the lattice (Fig. 1E,F). The localization of Kif18b–mRuby3 to the microtubule plus end was slightly reduced by the addition of MCAK and EB3 (Fig. S2C). This could be due to the Kif18b C-terminus engaging with EB3 and MCAK rather than the microtubule lattice. Indeed, we previously showed that the last 90 amino acids of Kif18b that contain two SxIP motifs increase the residence time of Kif18b at microtubule plus ends by 3-fold (McHugh et al., 2018). Thus, in our assay, Kif18b promotes the accumulation of both MCAK and EB3 proteins individually to the plus ends of microtubules. In the presence of both 50 nM $SNAP_{647}$–EB3 and 12.5 nM Kif18b–GFP, MCAK plus-end accumulation was further enhanced (Fig. 1E,F), indicating that, although MCAK interacts weakly with EB proteins (Montenegro Gouveia et al., 2010) and Kif18b (Fig. 1E,F), multivalent weak interactions of MCAK with both EB3 and Kif18b increase its accumulation to microtubule ends. The distribution of MCAK at the plus ends of microtubules varied upon addition of Kif18b or Kif18b and EB3, possibly reflecting different degrees of taper at the plus end of the taxol- and GMPCCP-stabilized microtubules that is induced by depolymerases (MCAK–Kif18b motor domain) and microtubule-stabilizing factors (Kif18b C-terminus–EB3) (McHugh et al., 2018; Montenegro Gouveia et al., 2010).

To test whether the Kif18b-dependent localization of MCAK to microtubule plus ends was specific to MCAK, we mixed the microtubule crosslinker PRC1–GFP (Subramanian et al., 2010) and Kif18b and incubated them with stabilized microtubules that were pre-immobilized on coverslips (Fig. S2D,E). No accumulation of

Journal of Cell Science (2023) 136, jcs260144. doi:10.1242/jcs.260144

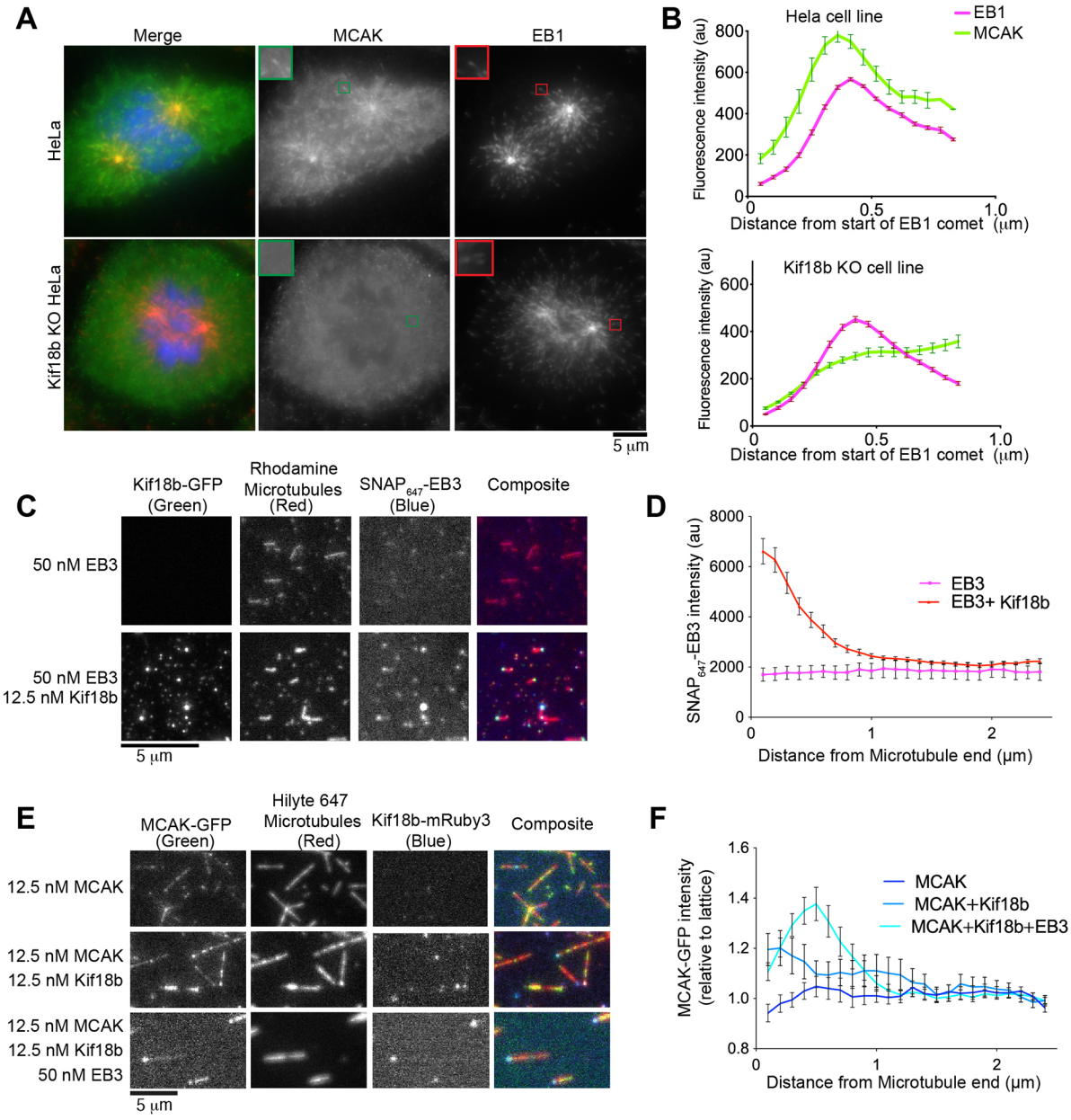

Fig. 1. Kif18b increases the localization of MCAK at microtubule plus ends. (A) Representative immunofluorescence images of MCAK (green) and EB1 (red) localization in HeLa and Kif18b-knockout (KO) Hela cells. Scale bar: 5 µm. (B) Quantification of EB1 and MCAK mean fluorescence intensity at astral microtubule plus ends (n=30 and 27, respectively), repeated three times from independent experiments. Mean and standard error of the mean (s.e.m.) are represented. (C,D) Kif18b binds to EB3 on GMPCPP microtubules. Representative images (C) of Kif18b–GFP and $SNAP_{647}$–EB3 on GMPCPP-stabilized Rhodamine-labelled microtubules. Scale bar: 5 µm. Quantification (D) of EB3 fluorescence intensity at the microtubule plus end in the presence (red, n=41) or absence (pink, n=44) of 12.5 nM Kif18b–GFP (indicated as mean±s.d.). (E,F) Kif18b and EB3 increase the plus-end localization of MCAK. Representative images (E) of MCAK–GFP (green) localization on taxol- and GMPCPP-stabilized microtubules. Scale bar: 5 µm. Quantification (F) of 12.5 nM MCAK–GFP fluorescence intensity (mean ±s.e.m.) at microtubule plus ends relative to the lattice, alone (dark blue, n=76), with 12.5 nM Kif18b–mRuby3 (blue, n=90) or with 12.5 nM Kif18b–mRuby3 and 50 nM $SNAP_{647}$–EB3 (cyan, n=116). au, arbitrary units. Kruskal–Wallis test at 0.2 µm: MCAK versus Kif18b+MCAK, P=0.0186; MCAK versus Kif18b+MCAK+EB3, P<0.0001. Images are representative of three independent experiments.

PRC1 at the ends of single microtubules was observed, confirming that the Kif18b-dependent delivery of MCAK and EB3 was specific. The presence of Kif18b at the ends of microtubules resulted in a small decrease in PRC1 intensity (Fig. S2E), perhaps due to competition for space on the lattice in this region. Our data indicate that Kif18b promotes EB3 and MCAK plus-end targeting and that Kif18b and EB3 proteins function cooperatively to facilitate microtubule plus-end accumulation of MCAK.

Kif18b targets the N-terminus of MCAK to microtubule plus ends

Previous work showed that in cells, Kif18b does not interact with a phosphomimetic mutant of MCAK, in which residues phosphorylated by Aurora kinases in the N-terminus of MCAK were mutated to glutamates (Tanenbaum et al., 2011). Thus, we hypothesized that MCAK interaction with Kif18b might be mediated by its N-terminus. To test this, we expressed the N-

Journal of Cell Science (2023) 136, jcs260144. doi:10.1242/jcs.260144

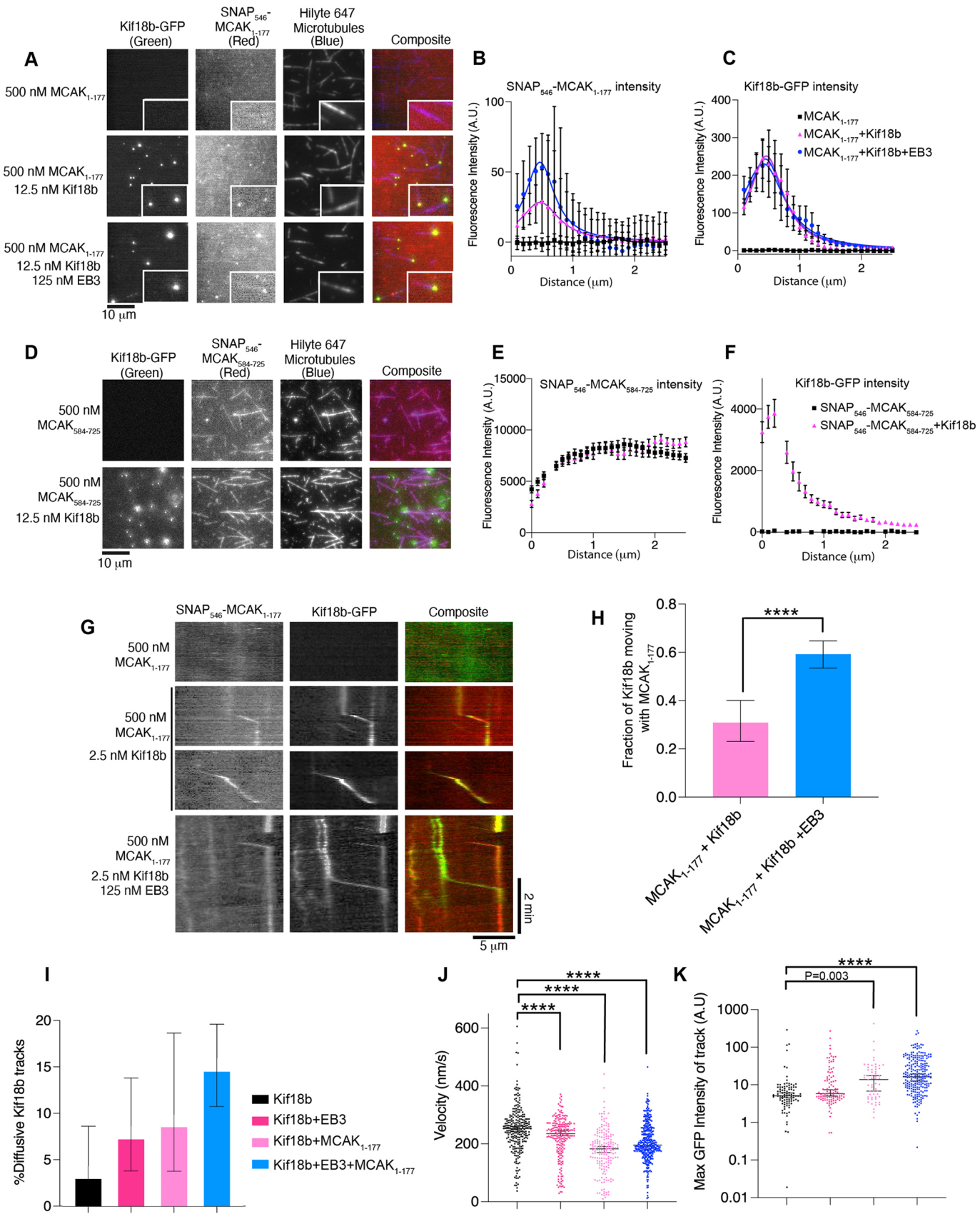

Fig. 2. See next page for legend.

Fig. 2. Single MCAK motors show increased lattice residency and directional movement in the presence of Kif18b. (A) Representative images of Kif18b–GFP, $SNAP_{546}$–$MCAK_{1–177}$, and unlabelled EB3 on GMPCPP-stabilized $HiLyte_{647}$-labelled microtubules. Scale bar: 10 µm. (B) Quantification of $SNAP_{546}$–$MCAK_{1–177}$ fluorescence intensity at the microtubule plus end (alone, black *n*=36), with 12.5 nM Kif18b–GFP (pink, *n*=43) or with 12.5 nM Kif18b–GFP and 125 nM EB3 (blue, *n*=28) (mean±s.e.m.). Kruskal–Wallis test at 0.5 µm: MCAK versus Kif18b+MCAK, *P*=0.0001; MCAK versus Kif18b+MCAK+EB3, *P*<0.0001. (C) Quantification of GFP fluorescence intensity at the microtubule plus end when MCAK alone is present (black, *n*=36), in the presence of 25 nM Kif18b–GFP (pink, *n*=43) and with 125 nM EB3+12.5 nM Kif18b–GFP (blue, *n*=28) (mean±s.e.m.). (D) Representative images of Kif18b–GFP and $SNAP_{546}$–$MCAK_{584–725}$ on GMPCPP-stabilized $HiLyte_{647}$-labelled microtubules. Scale bar: 10 µm. (E) Quantification of $SNAP_{546}$–$MCAK_{584–725}$ fluorescence intensity at the microtubule plus end alone (black, *n*=57) and in the presence of 12.5 nM Kif18b–GFP (pink, *n*=54) (mean±s.e.m.). (F) Quantification of GFP fluorescence intensity at the microtubule plus end when MCAK alone is present (black, *n*=57) or in the presence of 12.5 nM Kif18b–GFP (pink, *n*=54) (mean±s.e.m.). (G) Kymographs of 500 nM $SNAP_{546}$–$MCAK_{1–177}$ (red) alone, and with 2.5 nM Kif18b–GFP (green) in the presence or absence of 125 nM EB3 on GMPCPP-stabilized microtubules. Scale bars: 5 µm (horizontal) and 2 min (vertical). (H) Fraction of moving particles in the Kif18b–GFP channel that colocalize with particles moving in the $SNAP_{546}$–$MCAK_{1–177}$ channel with 500 nM $MCAK_{1–177}$, 2.5 nM Kif18b–GFP and with (blue, *n*=110) or without (pink, *n*=287) 250 nM EB3. Error bars represent the Wilson/Brown 95% c.i. Asterisks indicate Fisher's exact test significance value. ****P<0.0001. (I) Bar graph showing the fraction of Kif18b tracks displaying diffusive behaviour when Kif18b is alone (black, *n*=98), with EB3 (magenta, *n*=109), with $MCAK_{1–177}$ (pink, *n*=58) and with EB3 and $MCAK_{1–177}$ (blue, *n*=246). Error bars represent the Wilson/Brown 95% c.i. (J) The average velocity (mean±s.e.m.) of Kif18b–GFP motors for Kif18b–GFP alone (black, *n*=252), Kif18b–GFP with EB3 (magenta, *n*=216), Kif18b–GFP and $SNAP_{546}$–$MCAK_{1–177}$ with (pink, *n*=372) and without (blue, *n*=178) 125 nM EB3. Asterisks indicate ordinary one-way ANOVA with Tukey's post hoc test significance value. ****P<0.0001. (K) Scatter dot plot showing the distribution of GFP fluorescence intensity of Kif18b binding events for Kif18b alone (black, *n*=98), Kif18b+EB3 (magenta, *n*=107), Kif18b+$MCAK_{1–177}$ (pink, *n*=59) and Kif18b+EB3+$MCAK_{1–177}$ (blue, *n*=247). A.U., arbitrary units. Bars represent the median and 95% c.i. Asterisks indicate Kolmogorov–Smirnov test significance value. ****P<0.0001. Images are representative of three independent experiments.

terminus of MCAK ($MCAK_{1–177}$) and its C-terminus ($MCAK_{584–725}$) fused to SNAP labelled with Alexa Fluor 546 ($SNAP_{546}$). Alone, $SNAP_{546}$–$MCAK_{1–177}$ did not bind to the microtubules, nor did it bind Kif18b in solution (Fig. 2A–C; Fig. S1E). In the presence of 12.5 nM Kif18b, we observed an enrichment of $SNAP_{546}$–$MCAK_{1–177}$ at the plus ends of GMPCPP-stabilized microtubules, where Kif18b accumulated (Fig. 2A–C). This was further enhanced by the addition of EB3. In contrast, the C-terminus of MCAK ($MCAK_{584–725}$) uniformly decorated the microtubule lattice both in the presence and absence of Kif18b (Fig. 2D–F). These results indicate that microtubule-bound Kif18b interacts specifically with the N-terminus of MCAK.

Kif18b increases directional MCAK movement along the lattice

We next tested whether Kif18b can transport MCAK along microtubules using $SNAP_{546}$–$MCAK_{1–177}$. We observed $SNAP_{546}$–$MCAK_{1–177}$ moving with Kif18b–GFP along GMPCPP-stabilized microtubules in the absence and presence of unlabelled EB3 by two-colour fluorescence imaging (Fig. 2G). A fraction of Kif18b motors displayed co-localization with the N-terminal fragments of MCAK. This was increased in the presence of EB3, which interacts with both MCAK and Kif18b. In the presence of EB3, most Kif18b motors co-localized with the N-terminal fragments of MCAK (Fig. 2H). Kif18b displayed a modest increase in diffusive behaviour in the presence of EB3 and/or MCAK N-terminus, indicating that the binding of cargos impacts the behaviour of Kif18b on the lattice (Fig. 2I). Additionally, the velocity of Kif18b decreased when bound to the N-terminus of MCAK and/or EB3 (Fig. 2J). Kif18b–GFP remained dimeric on microtubules when alone or in the presence of EB3 (Fig. 2K; Fig. S3A,B). However, there was an increase in the fluorescence intensity of Kif18b–GFP moving on microtubules in the presence of the MCAK N-terminus, indicating potential oligomerization (Fig. 2K). Together, our work indicates that Kif18b interacts with MCAK through its N-terminus and that this interaction is further stabilized by EB3, which binds both Kif18b and MCAK. Kif18b transports the N-terminus of MCAK towards the plus end of the microtubule lattice, while MCAK also influences the motile properties of Kif18b.

To test whether Kif18b can promote transport of full-length MCAK, we then imaged low concentrations of labelled MCAK–GFP on stable microtubules to record single-molecule events using fast imaging (10 frames per second) (Fig. S3C). MCAK alone diffused on microtubules – we measured a diffusion coefficient of 5510±734 nm^2/s (estimated by the least square fit; indicated as gradient±95% c.i.) (Fig. S3D) – and remained bound to the lattice for 1.3±0.5 s on average (Fig. S3E). In the presence of 10 nM Kif18b, MCAK lattice residency increased to 2.4±0.2 s and MCAK was more diffusive with a 4-fold increase in diffusion coefficient to 24,082±1478 nm^2/s (Fig. S3C–E). At 10 nM Kif18b and the sub-nanomolar concentrations of MCAK–GFP that are required for single-molecule imaging, we saw MCAK accumulating at the microtubule ends. Although we could not distinguish the polarity of the stable microtubules, we could infer that MCAK was accumulating at microtubule plus ends, where the Kif18b concentration would have been at its highest, given the plus-end accumulation of Kif18b (Fig. S3C) (McHugh et al., 2018). We also observed events of directional movement of MCAK, often at rates of around 300 nm/s, corresponding to those seen for single Kif18b motors (McHugh et al., 2018) (Fig. S3C). This, when combined with our data for $SNAP_{546}$–$MCAK_{1–177}$ (Fig. 2G), indicates that the accumulation of MCAK at the plus ends of microtubules in the presence of Kif18b is due, at least in part, to direct plus-end-directed transport of MCAK as a cargo of Kif18b. Multivalent interactions between Kif18b, EB3 and MCAK proteins in the context of the microtubule create an Kif18b–MCAK–EB3 plus-end-localized network.

The C-terminus of Kif18b stabilizes microtubules

We previously showed that the C-terminus of Kif18b binds to microtubules and enables Kif18b to remain bound to the plus ends of both stable and dynamic microtubules (McHugh et al., 2018). It also opposes the weak depolymerase activity of Kif18b, similarly to budding yeast kinesin-8 Kip3 (Su et al., 2011). We therefore tested whether Kif18b interfered with MCAK-induced depolymerization of stable microtubules through its microtubule-binding C-terminus. It is important to note that full-length Kif18b–GFP accumulated at microtubule plus ends but did not depolymerize GMPCPP-stabilized microtubules, and that MCAK caused slow microtubule depolymerization of GMPCPP-stabilized microtubules from both ends rather than inducing catastrophe (Fig. 3A). This slow depolymerization of microtubules allowed us to probe how MCAK and Kif18b can work together at microtubule ends (Fig. 3A–E) and image single molecules of MCAK on microtubules (Fig. 3F). In the presence of 25 nM MCAK–GFP, the addition of Kif18b caused a decrease in depolymerization of microtubule ends that was dependent on Kif18b concentration and

Journal of Cell Science (2023) 136, jcs260144. doi:10.1242/jcs.260144

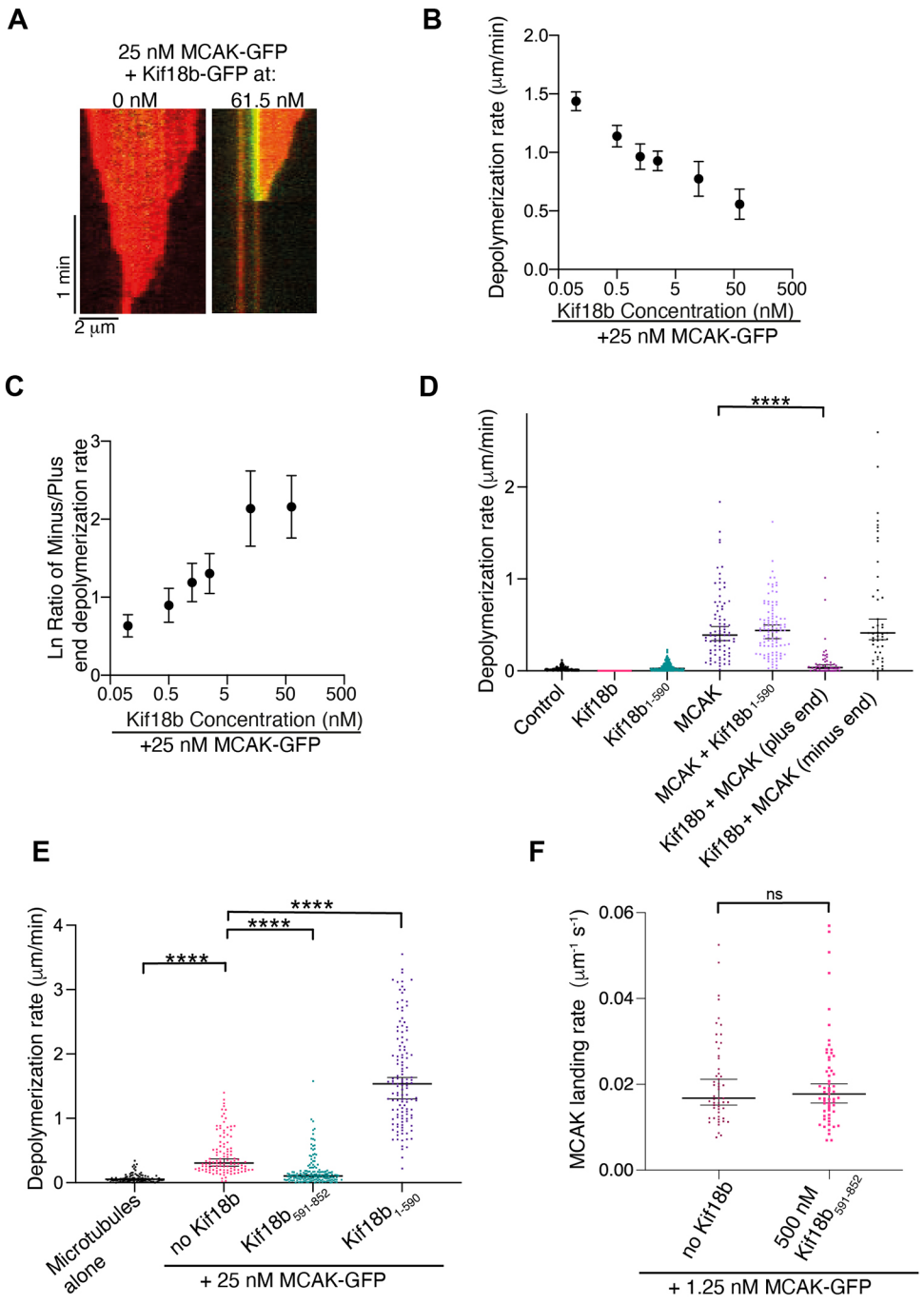

Fig. 3. The C-terminal tail of Kif18b opposes MCAK-mediated microtubule depolymerization. (A) Example kymographs showing the depolymerization of GMPCPP microtubules by 25 nM MCAK–GFP in the presence (right) and absence (left) of 61.5 nM Kif18b–GFP. Scale bars: 1 min (vertical) and 2 µm (horizontal). Images are representative of three independent experiments. (B) Increasing Kif18b–GFP concentrations led to lower microtubule depolymerization rates mediated by 25 nM MCAK–GFP. Data are represented as mean±s.e.m. n=270. Spearman correlation of −1 with P=0.004, showing a monotonic relationship between microtubule depolymerization rate and Kif18b concentration. (C) Natural logarithmic ratio of minus-/plus-end depolymerization rate with increasing Kif18b concentrations in the presence of 25 nM MCAK–GFP. Data are represented as mean±s.e.m. n=270. Spearman correlation of +1 with a P=0.004, showing a monotonic relationship between the ratio of minus-/plus-end depolymerization rate and Kif18b concentration. (D) Depolymerization rates for GMPCPP-stabilized microtubules alone (n=110), with 25 nM Kif18b–GFP (n=74), with 25 nM Kif18b$_{1–590}$–GFP (n=272), with 25 nM MCAK–GFP (n=82), with 25 nM Kif18b$_{1–590}$–GFP and 25 nM MCAK–GFP (n=104) and with 25 nM Kif18b–GFP and 25 nM MCAK–GFP (plus- and minus-end rates) (n=49). Bars represent the median and 95% c.i. Asterisks indicate an ordinary Kruskal–Wallis test significance value when comparing depolymerization rates in the presence of MCAK or with MCAK+Kif18b constructs. ****P<0.0001. Also see Table S1. (E) Depolymerization rates for GMPCPP-stabilized microtubules alone (n=94), with 25 nM MCAK (n=113), with 25 nM MCAK and 250 nM Kif18b$_{1–590}$–GFP (absolute concentration of 500 nM, n=165) and with 25 nM MCAK and 500 nM Kif18b$_{591–852}$–GFP (n=127) Asterisks indicate an ordinary Kruskal–Wallis test significance values. ****P<0.0001. (F) MCAK landing rate on microtubules with 1.25 nM MCAK–GFP in the presence or absence of 500 nM Kif18b$_{591–852}$ (n=53 and 59, respectively) (Table S1). Bars represent the median and 95% c.i. Kolmogorov–Smirnov test, P=0.9754. ns, not significant.

specific to the plus end where Kif18b–GFP accumulated (Fig. 3A,B). This led to an asymmetry in plus- and minus-end depolymerization rates, proportional to the concentration of Kif18b (Fig. 3C). In the presence of 25 nM MCAK and 25 nM full-length Kif18b, the rate of the microtubule plus-end depolymerization was severely reduced to 0.036 µm/min, whereas the free minus-end depolymerization rate was similar to that with MCAK alone (0.390 µm/min) (Fig. 3D; Table S1). We found that in the presence of MCAK and a C-terminally truncated Kif18b$_{1–590}$–GFP, the microtubule depolymerization rate was similar to the rate in the presence of MCAK alone, indicating that the plus-end localization of the C-terminus of Kif18b interfered with MCAK-mediated depolymerization of stable microtubules. We then used a high concentration of Kif18b truncation mutants to compensate for their inability to accumulate at microtubule plus ends (Fig. 3E; Table S2). The addition of 250 nM Kif18b$_{1–590}$ displayed strong depolymerase activity, as previously shown (McHugh et al., 2018). The addition of 500 nM Kif18b$_{591–852}$ (which is monomeric and corresponds to the concentration of molecules for 250 nM dimeric Kif18b) significantly reduced the rate of MCAK-induced depolymerization, without affecting the landing rate of MCAK, defined as the number of MCAK motors binding to the lattice (µm^{-1}/s) (Fig. 3F; Table S3). This indicates that the C-terminus of Kif18b further stabilizes the GMPCCP-stabilized microtubule lattice against MCAK depolymerase activity, rather than preventing MCAK association with the microtubules.

Journal of Cell Science (2023) 136, jcs260144. doi:10.1242/jcs.260144

On dynamic microtubules, addition of 500 nM of the C-terminus of Kif18b increased the growth rate of microtubules (Fig. S4A), consistent with a role in microtubule lattice stabilization. However, it did not impact the catastrophe frequency or overall microtubule length (Fig. S4B,C). In the presence of 12.5 nM MCAK and 500 nM Kif18b$_{591–852}$, the growth rate of microtubules remained elevated (Fig. S4D), and the catastrophe frequency and overall microtubule length were largely unchanged (Fig. S4E,F). Thus, in the context of dynamic microtubules, the C-terminus of Kif18b alone did not stabilize microtubules against MCAK activity. Overall, stabilized microtubules allowed the accumulation of Kif18b and MCAK at microtubule plus ends where Kif18b mediated a stabilizing effect. In contrast, on dynamic microtubules, catastrophe led to loss of motors associated with the depolymerizing end, lessening any stabilizing role the C-terminus of Kif18b might have had. Most kinesin-8 proteins appear to use their C-terminal domains to counteract the activity of their microtubule-depolymerizing motor domains, but most importantly to facilitate their plus-end targeting (Stumpff et al., 2011; Su et al., 2013; Su et al., 2011).

Effect of Kif18b, EB3 and MCAK on microtubule dynamics

We then sought to define the properties of the Kif18b–MCAK–EB3 network on dynamic microtubules. We first analysed the effects of MCAK alone on dynamic microtubules using GMPCPP-stabilized seeds with microtubules growing from them. We observed that MCAK acts as a strong catastrophe factor (Fig. 4A–C; Table S4). Increasing MCAK concentration from 0 to 25 nM led to high catastrophe frequencies, ranging from 0.34 min^{-1} to 1.1 min^{-1}, respectively (Fig. 4A,B; Table S4), as previously reported (Gardner et al., 2011). The extension lengths of microtubules were significantly shorter upon increasing concentrations of MCAK, corresponding to 2.68±0.21 and 1.51±0.14 µm for 12.5 and 25 nM MCAK, respectively, whereas the microtubule extension lengths alone were 3.85±0.69 µm (indicated as median±95% c.i.) (Fig. 4C; Table S4).

We next analysed whether microtubule dynamics in the presence of MCAK were altered by the addition of EB3 (Fig. 4D–F). In the presence of 12.5 nM MCAK, catastrophe frequency increased significantly from 1.02 to 1.16 min^{-1} upon the addition of 25 nM EB3 (Fig. 4E). However, there were no major changes in microtubule lengths between conditions in which MCAK or MCAK and EB3 were used (Fig. 4F; Table S5). In addition, we could see little enrichment of MCAK at microtubule plus ends under these conditions (Fig. 4D). This can be explained by the dissociation constant of EB proteins with MCAK being in the micromolar range of 10 µM (Buey et al., 2012). It was nevertheless possible to see robust EB3-dependent MCAK tracking the growing ends of microtubules when higher concentrations of EB3 and MCAK were used. However, the microtubule seeds had to be additionally stabilized with taxol to counteract MCAK depolymerase activity as seen in Montenegro Gouveia et al. (2010) and Fig. S5A. Thus, we did not quantify microtubule dynamics under these conditions. In total, these data indicate that at low nanomolar concentrations, MCAK depolymerizes microtubules independently of EB3.

We next tested how Kif18b and MCAK influence microtubule dynamics when combined. We have previously shown that Kif18b only has a modest effect on microtubule dynamics, increasing catastrophe frequency and growth rate, thereby leading to slightly reduced microtubule extension lengths (McHugh et al., 2018). Using 12.5 nM of each dimeric motor, we compared the effect of the motors alone and in combination (Fig. 4G). The addition of 12.5 nM MCAK increased catastrophe frequency (Fig. 4H; Table S6), and this occurred to a greater extent than for Kif18b (Fig. 4G,I). In the presence of both MCAK and Kif18b, catastrophe frequency further increased (Fig. 4I), whereas microtubule length was reduced when both Kif18b and MCAK were present (Fig. 4G,I).

Kif18b, EB3 and MCAK track the growing ends of microtubules together to increase catastrophe frequency and decrease microtubule length

We next defined the properties of the Kif18b–MCAK–EB3 network on dynamic microtubules. When using 12.5 nM MCAK, 12.5 nM Kif18b and 25 nM EB3, no dynamic microtubule extensions were seen (Fig. S5B), indicating that the combination of Kif18b, EB3 and MCAK had a dramatic effect on microtubules, which could not equate to the sum of their individual activities. To enable quantification of this effect, we decreased the amount of MCAK in our assays to 5 nM, while keeping 12.5 nM Kif18b and 25 nM EB3, and imaged the microtubule extensions grown from GMPCPP-stabilized seeds in the presence of 12 µM tubulin. A significant effect was seen in the presence of all three proteins on both catastrophe frequency and microtubule extension lengths. Catastrophe frequency was found to be the highest and, conversely, the dynamic microtubule extensions were the shortest under these conditions (Fig. 5A,B; Table S7). There was a 2-fold increase in catastrophe frequency from 0.34 min^{-1} for treatment with MCAK and EB3 to 0.74 min^{-1} for treatment with MCAK, EB3 and Kif18b (Fig. 5A). Overall, this resulted in a 1.8-fold reduction in the length of dynamic extensions when Kif18b was added to EB3 and MCAK, with the microtubules remaining dynamic and short (Fig. 5B,C; Table S7). We then imaged the three proteins simultaneously using microtubule seeds that were doubly stabilized with taxol and GMPCPP, prepared as in Montenegro Gouveia et al. (2010) (Fig. 5D). As expected, MCAK mostly diffused on the lattice, whereas EB3 tracked the growing ends of microtubules, and Kif18b exhibited processive behaviour walking towards microtubule plus ends. In the presence of Kif18b, there was a slight enrichment of MCAK towards the growing plus end of microtubules (white arrows, Fig. 5D) and plus-end-directed processive events could be seen with MCAK–GFP moving at 296 nm/s, similar to the results we previously reported for Kif18b alone (Fig. S5C,D) (McHugh et al., 2018). When all three proteins, Kif18b, MCAK and EB3, were present, MCAK tracked the plus ends of growing microtubules along with Kif18b and EB3 (Fig. 5D). The addition of EB3 increased the proportion of processive plus-end-directed MCAK–GFP motors, although the majority (>90%) of MCAK–microtubule-binding events were diffusive (Fig. S5E). When the protein concentration was slightly higher, Kif18b-mediated transport events of EB3 and MCAK towards the microtubule ends were more readily apparent (Fig. 5E; Movie 1). These complexes formed bright clusters of multiple proteins, indicating assembly of the Kif18b–MCAK–EB3 network, and were transported to the plus ends by Kif18b. Together, the Kif18b–MCAK–EB3 network cooperates in an integrated manner to dramatically increase microtubule catastrophe in mitosis.

DISCUSSION

Microtubule dynamics dramatically increase at mitotic onset when microtubules shorten to remodel the microtubule cytoskeleton and assemble a bipolar spindle (Belmont et al., 1990; Piehl and Cassimeris, 2003). This change in microtubule length is attributed mainly to an increase in the catastrophe frequency (Belmont et al., 1990). Although Kif18b alone is a weak microtubule depolymerase

Journal of Cell Science (2023) 136, jcs260144. doi:10.1242/jcs.260144

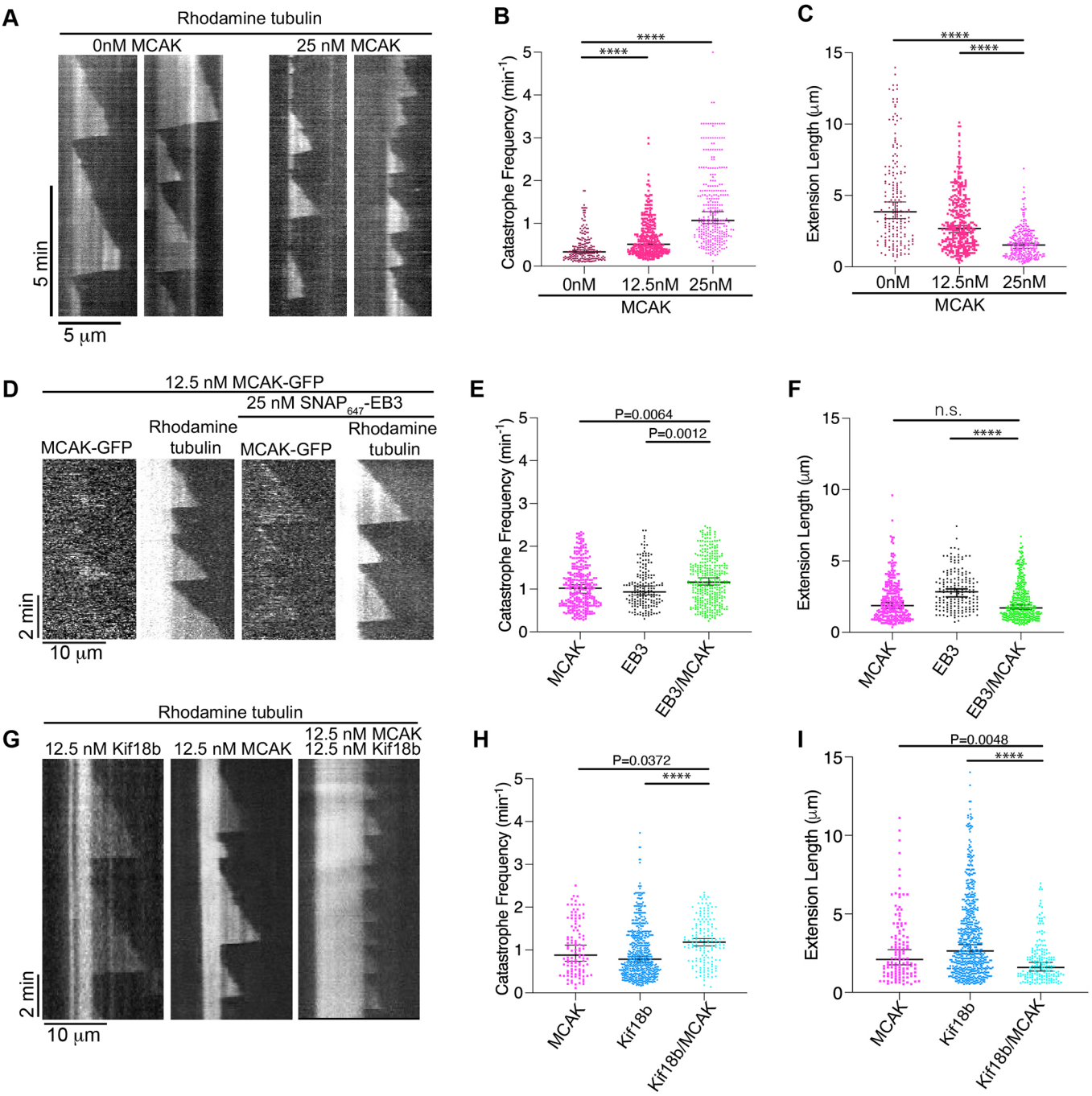

Fig. 4. MCAK and Kif18b increase microtubule catastrophe frequency and decrease microtubule length. (A) Representative kymographs of dynamic microtubules in the presence of 0 nM and 25 nM MCAK–GFP with 12 µM tubulin. Scale bars: 5 µm (horizontal) and 5 min (vertical). (B,C) Microtubule catastrophe frequency (B) and length of dynamic microtubule extensions (C) with increasing MCAK concentrations. *n*>184 for each condition; values (median and 95% c.i.) are given in Table S1. We were unable to consistently detect microtubule growth events that occurred for less than 25 s, so these data were removed from our analysis. Asterisks indicate Kruskal–Wallis test significance values; ****P<0.0001. (D) Representative kymographs of dynamic microtubules in the presence of 12.5 nM MCAK–GFP and 25 nM $SNAP_{647}$–EB3 with 7 µM tubulin. Scale bars: 10 µm (horizontal) and 2 min (vertical). (E,F) Microtubule catastrophe frequency (E) and length of dynamic microtubule extensions (F) in the presence of 12.5 nM MCAK and 25 nM $SNAP_{647}$–EB3. *n*>175 for all conditions; values (median and 95% c.i.) are given in Table S1. Asterisks indicate Kruskal–Wallis test significance values: n.s., not significant; ****P<0.0001. (G) Representative kymographs of dynamic microtubules in the presence of 12.5 nM MCAK–GFP and/or 12.5 nM Kif18b–mRuby3 with 7 µM tubulin. Scale bars: 10 µm (horizontal) and 2 min (vertical). (H,I) Microtubule catastrophe frequency (H) and length of dynamic microtubule extensions (I) in the presence of 12.5 nM MCAK–GFP and/or 12.5 nM Kif18b–mRuby3. *n*>110 for all conditions; values (median and 95% c.i.) are given in Table S1. Asterisks indicate Kruskal–Wallis test significance values; ****P<0.0001. Images are representative of three independent experiments.

in vitro, it is a major microtubule depolymerization factor in mitosis once released from the nucleus (Lee et al., 2010). In the absence of Kif18b or MCAK, mitotic microtubules remain long, leading to spindle assembly and positioning defects in humans (McHugh et al., 2018; Rankin and Wordeman, 2010; Stout et al., 2011; Tanenbaum et al., 2011; van Heesbeen et al., 2016). Here, we show

Journal of Cell Science (2023) 136, jcs260144. doi:10.1242/jcs.260144

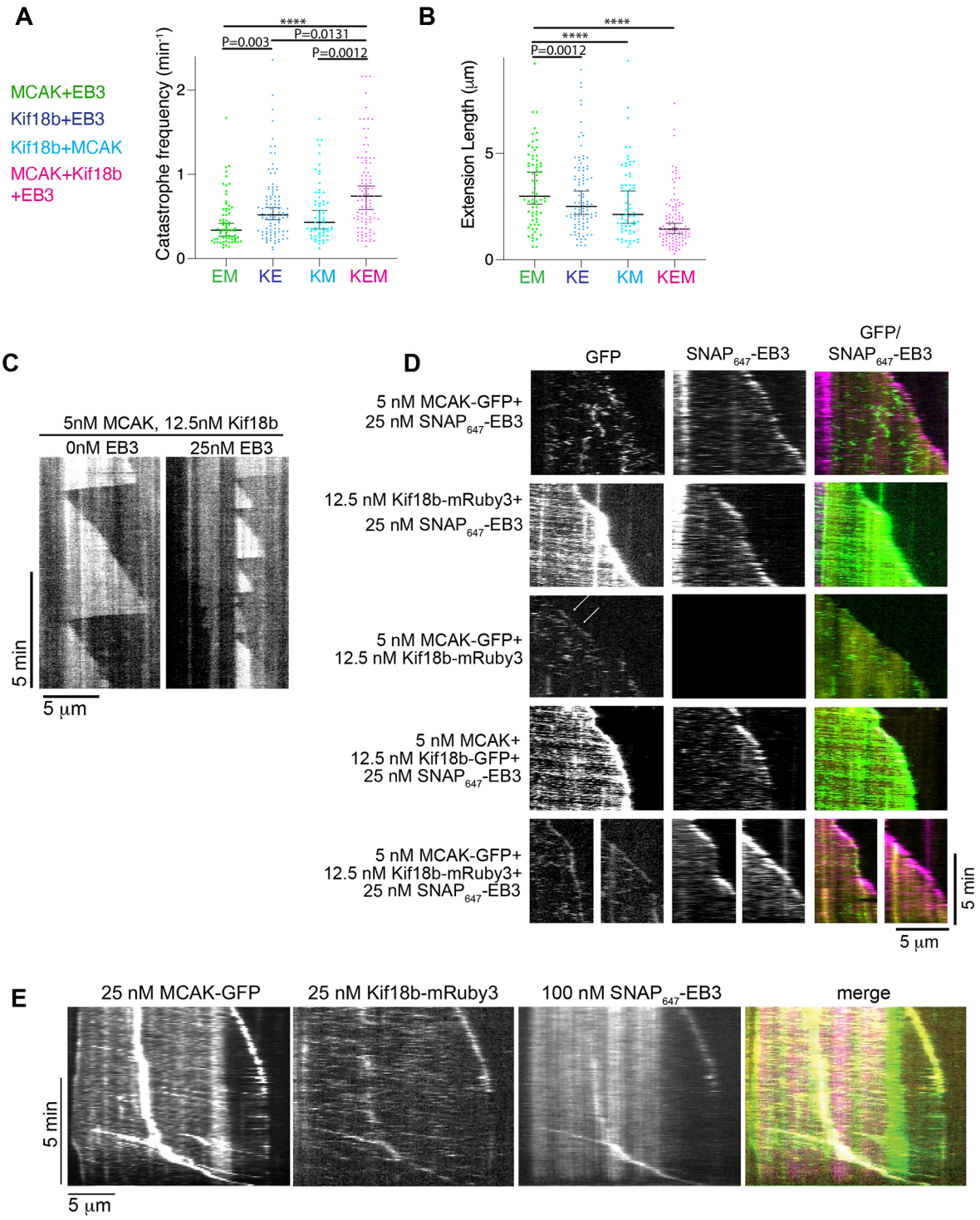

Fig. 5. Kif18b-dependent delivery of MCAK and EB3 to microtubule plus ends leads to high catastrophe frequencies and shortening of microtubule length. (A,B) Microtubule catastrophe frequency (A) and length of dynamic microtubule extensions (B) in the presence of 5 nM MCAK–GFP, 12.5 nM Kif18b–mRuby3 and/or 25 nM $SNAP_{647}$–EB3. EM, EB3+MCAK; KE, Kif18b+EB3; KM, Kif18b+MCAK; KEM, Kif18b+EB3+MCAK. Details on *n* values, median and 95% c.i. are given in Table S1. Asterisks indicate Kruskal–Wallis test significance values; ****P<0.0001. (C) Representative kymographs of dynamic microtubules in the presence of 5 nM MCAK–GFP and 12.5 nM Kif18b–mRuby3, and with 0 nM or 25 nM $SNAP_{647}$–EB3 with 12 µM tubulin. Scale bars: 5 min (vertical) and 5 µm (horizontal). (D) Representative kymographs of dynamic microtubules in the presence of 5 nM MCAK–GFP or His–MCAK, 12.5 nM Kif18b–mRuby3 or Kif18b–GFP and 25 nM $SNAP_{647}$–EB3 with 12 µM tubulin. Scale bars: 5 min (vertical) and 5 µm (horizontal). Seeds were stabilized with GMPCPP and taxol, washed with ten volumes of BRB80 before 12 µM free tubulin and the protein mix was added. Note that residual taxol stabilizes the lattice. (E) Representative kymographs of dynamic microtubules in the presence of 25 nM MCAK–GFP (green), 25 nM Kif18b–mRuby3 (yellow) and 100 nM $SNAP_{647}$–EB3 (magenta) with 12 µM tubulin. Scale bars: 5 min (vertical) and 5 µm (horizontal). Seeds were stabilized with GMPCPP and taxol, the seeds were washed with five volumes of BRB80 before 12 µM free tubulin and the protein mix was added. Note that residual taxol stabilizes the lattice. Images are representative of three independent experiments.

Journal of Cell Science (2023) 136, jcs260144. doi:10.1242/jcs.260144

mechanistically how MCAK, Kif18b and EB3 cooperate to increase the catastrophe frequency of microtubules. Using single-molecule imaging and *in vitro* reconstitution, we find that Kif18b can transport MCAK via interactions with both the MCAK N-terminus and EB3 to microtubule plus ends, where they promote microtubule catastrophe. It is clear from our data that missing any one component of the Kif18b–MCAK–EB3 network results in reduced capability for limiting microtubule length.

Our data challenge previous models that postulate that MCAK uses diffusion alone to reach microtubule ends (Cooper et al., 2010; Helenius et al., 2006). Although one-dimensional diffusion on the microtubule lattice is an efficient way to reach a microtubule end over short distances, diffusion is not necessarily an efficient way to reach specifically the plus end of a microtubule in a cell. The diffusion rate of MCAK was calculated to be 5510 nm^2/s with a residence time of 1.3 s. This would mean that a single motor on average explores just 84 nm of the microtubule lattice with each encounter. In the presence of Kif18b, both MCAK diffusion and residence time increase: MCAK would diffuse an average of 240 nm, thereby increasing the probability MCAK would reach or get close to a microtubule plus end. However, diffusion alone does not explain how MCAK localizes primarily to microtubule plus ends on crowded and long microtubules in cells.

The molecular structure of the Kif18b–MCAK–EB3 network remains poorly understood. MCAK binding to both Kif18b and EB proteins has been shown to be weak (Fig. S1E) (Buey et al., 2012). Given that Kif18b and MCAK have large regions of low complexity (Fig. S1B,C), it is likely that they assemble as higher oligomers through weak multivalent interactions within their unstructured domains on the microtubules (Fig. 5E), offering many binding sites to EB3.

The localization of endogenous MCAK at microtubule plus ends in interphase cells is barely detectable using immunofluorescence, prompting most studies to use fluorescently labelled MCAK (Moore et al., 2005). Endogenous MCAK has only been observed in mitosis and MCAK localization is dependent on the Kif18b and EB proteins (Fig. 1) (Tanenbaum et al., 2011), suggesting that less MCAK is present at the ends of interphase microtubules. Indeed, similarly to Kif18b, the most striking effects of the kinesin-13 proteins are on mitotic microtubules. Our work demonstrates that Kif18b, EB3 and MCAK collectively form a protein network at dynamic microtubule plus ends at very low concentrations of each component. At these plus ends, Kif18b plays a critical role as an integration platform to modulate the depolymerase activity of the network. Kif18b enhances the accumulation of MCAK on the lattice and at microtubule ends and delivers MCAK and EB3 proteins to the microtubule ends (Fig. 6), where they work together in an integrated manner to increase microtubule catastrophe. The unique and potent properties of the network cannot be imparted to the sum of the individual components (Fig. 5).

Two distinct populations of Kif18b decorating astral microtubule plus ends have been reported; one population of Kif18b colocalizes with EB1, whereas the other population precedes EB1 at the plus end of the microtubules (Shin et al., 2015). Kif18b is a fast motor, with a speed of 350 nm/s *in vitro* and up to 700 nm/s *in vivo* (McHugh et al., 2018; Tanenbaum et al., 2014), faster than microtubule growth speed that is around 200–250 nm/s (Sironi et al., 2011). Thus, Kif18b can reach the growing end of a microtubule and accumulate there using its C-terminal microtubule-binding tail independently of EB proteins (McHugh et al., 2018). Indeed, small regions at the growing ends of microtubules were found to be EB-free (Maurer et al., 2014) and lacked lateral

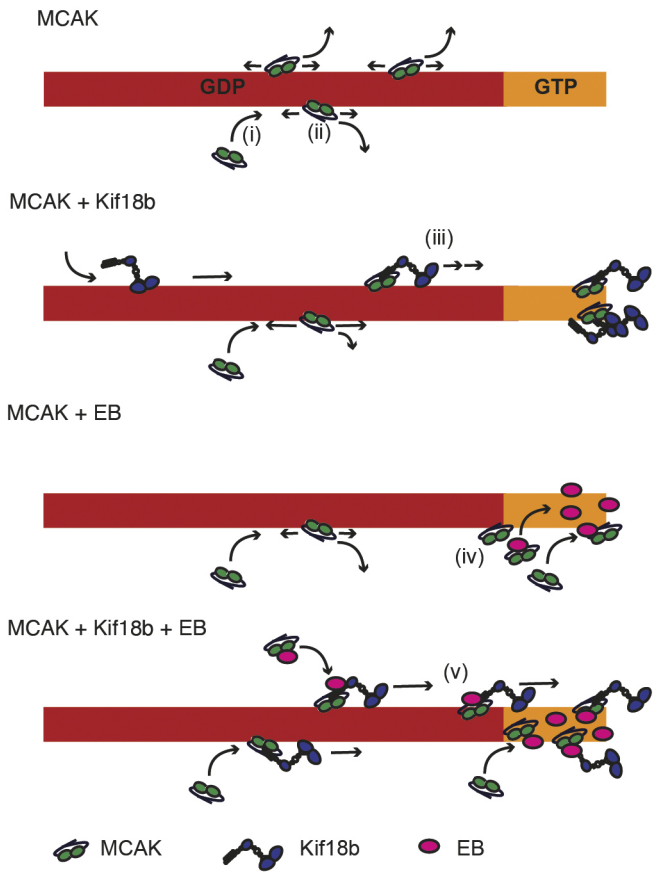

Fig. 6. Model of the Kif18b–MCAK–EB network at dynamic microtubule ends. MCAK alone binds to the microtubule lattice (indicated in red) and diffuses for short distances before detaching (ii). Few MCAK motors reach the microtubule end (indicated in orange). In the presence of Kif18b, MCAK transport occurs (iii). This leads to more MCAK arriving at the microtubule ends. MCAK also binds to EB proteins (iv), that are binding and exchanging at the GTP cap of microtubules. This enables the accumulation of MCAK to microtubule plus ends (iv). When both EB and Kif18b proteins are present, MCAK can bind EB and Kif18b at the microtubule plus ends or form a tripartite complex that can be transported to microtubule ends by Kif18b. As all proteins are dimeric, they can form a network of interactions at microtubule plus ends where they accumulate and promote microtubule depolymerization (v).

stabilization of protofilaments (McIntosh et al., 2018). It is possible that Kif18b brings MCAK and EB3 to the terminal tubulin dimers of microtubules where tubulin is assembled into single protofilaments but is not yet closed, to promote depolymerization. There, the Kif18b–MCAK–EB3 complex could efficiently depolymerize microtubule growing ends before they have been stabilized through lateral contacts of protofilaments, to avoid an additional energy barrier to depolymerization.

Importantly, each interaction within this Kif18b–MCAK–EB3 network is individually regulated by mitotic phosphorylation, a rapid and reversible post-translational modification (Tanenbaum et al., 2011; McHugh et al., 2018). Additionally, Kif18b is confined to the nucleus before mitosis and irreversibly degraded at the end of mitosis. Thus, the integrity and activity of this depolymerizing network is tightly regulated to allow for spatial, local and temporal regulation of microtubule dynamics during mitosis. It would be interesting to define whether Kif18b also delivers other microtubule-associated proteins with low-complexity domains to plus ends through interactions with its unstructured C-terminus. Finally, our work highlights the importance of studying motors not only in isolation but

examining their collective behaviour and the underlying emergent function. How cargos influence motor activity remains a poorly understood phenomenon. Rather than having a microtubule motor that provides transport to passive cargos, we reveal here how the three components of the mitosis-specific Kif18b–MCAK–EB3 network, two of which are motors, act in an integrated manner to provide increased depolymerization of microtubule plus ends with temporal and spatial layers of control.

MATERIALS AND METHODS

Cloning

Plasmids made for this study are summarized in Table S8. The Sf9 insect cell expression constructs for producing full-length human Kif18b–GFP, Kif18b$_{1–590}$–GFP and MCAK–GFP with a C-terminal 6×His have been described elsewhere (McHugh et al., 2018; Talapatra et al., 2015). For Kif18b–mRuby3–His, Kif18b was cloned into the pFL–mRuby3–His vector [constructed by inserting mRuby3–His6 into pFL (Addgene #110739)] using restriction enzymes. Kif18b$_{591–852}$ was cloned into pET3aTr (Addgene #64008) with an N-terminal 6×His. MCAK$_{1–177}$ and MCAK$_{584–725}$ were cloned into the pST50Trc1-HISNDHFR vector (Addgene #63940). EB3 was cloned into the pET3aTr vector containing a His, or the pST50Trc1-HISNDHFR vector containing His–TEV–SNAP or His–GFP tags. The pFL-His–TEV–GFP–PRC1 plasmid was a gift from Tarun Kapoor, Rockefeller University, NY and is described in Subramanian et al. (2010). mRuby3 was synthesized after codon optimization for expression in insect cells by GeneArt, Thermo Fisher Scientific. The DNA sequence for mRuby3 is as follows:

5′-ATGGTGTCTAAGGGCGAAGAGCTGATCAAGGAAAATATGC-GTATGAAGGTGGTCATGGAAGGTTCGGTCAACGGCCACCAATT-CAAATGCACAGGTGAAGGAGAAGGCAGACCGTACGAGGGAGT-GCAAACCATGAGGATCAAAGTCATCGAGGGAGGACCCCTGCCA-TTTGCCTTTGACATTCTTGCCACGTCGTTCATGTATGGCAGCCGT-ACCTTTATCAAGTACCCGGCCGACATCCCTGATTTCTTTAAACA-GTCCTTTCCTGAGGGTTTTACTTGGGAAAGAGTTACGAGATACG-AAGATGGTGGAGTCGTCACCGTCACGCAGGACACCAGCCTTGA-GGATGGCGAGCTCGTCTACAACGTCAAGGTCAGAGGGGTAAAC-TTTCCCTCCAATGGTCCCGTGATGCAGAAGAAGACCAAGGGTT-GGGAGCCTAATACAGAGATGATGTATCCAGCAGATGGTGGTCT-GAGAGGATACACTGACATCGCACTGAAAGTTGATGGTGGTGGC-CATCTGCACTGCAACTTCGTGACAACTTACAGGTCAAAAAAGAC-CGTCGGGAACATCAAGATGCCCGGTGTCCATGCCGTTGATCACC-GCCTGGAAAGGATCGAGGAGAGTGACAATGAAACCTACGTAGT-GCAAAGAGAAGTGGCAGTTGCCAAATACAGCAACCTTGGTGGT-GGCATGGACGAGCTGTACAAG-3′.

Cell culture

HeLa cells (93021013, Sigma-Aldrich, USA) were used and maintained in Dulbecco's Modified Eagle Medium (DMEM, Lonza) supplemented with fetal bovine serum (FBS; Thermo Fisher Scientific), glutamine and penicillin-streptomycin (15140122; Thermo Fisher Scientific) at 37°C in a humidified atmosphere with 5% CO_2. The generation of the Kif18b-knockout cell line is described in McHugh et al. (2018). Cells were purchased from American Type Culture Collection (ATCC) and were checked monthly for mycoplasma contamination (MycoAlert detection kit, Lonza).

Immunofluorescence and microscopy

Cells were washed in PBS and fixed in 3.8% formaldehyde in PHEM buffer (60 nM PIPES, 25 mM HEPES, 10 mM EGTA, 2 mM $MgSO_4$, pH 7.0) for 10 min. Immunofluorescence in human cells was performed using an antibody against mouse EB1 (610535; BD transduction laboratories, USA; 1:400) and a custom rabbit MCAK antibody (1:500 or 1:1000). The MCAK antibody, raised against GFP–MCAK, was generated by Eurogentec, Belgium, using the Speedy program. Over time, the antibody became rapidly unstable and non-specific. Images were acquired using a DeltaVision core microscope (bought from Applied Precision, Imsol, UK) with a 100× lens (NA: 1.4) equipped with a CoolSnap HQ2 CCD camera (Teledyne Photometrics, USA). 10–20 *z*-sections were acquired at 0.2–0.5 µm. Comet intensities were quantified as previously described (McHugh et al., 2018). Experiments were repeated three times independently.

Protein expression and purification

Kif18b and MCAK proteins were expressed using a baculovirus expression system; Sf9 cells were infected with the virus for each construct for 60–72 h. His–Kif18b$_{591–852}$, His–SNAP–MCAK$_{1–177}$, His–SNAP–MCAK$_{584–725}$, His–EB3 and His–GFP–PRC1 proteins with the His$_6$ tag cleavable with the 3C protease were expressed in BL21 CodonPlus *Escherichia coli* cells overnight at 18°C. His-tagged Kif18b and MCAK proteins were purified as previously described (Talapatra et al., 2015). His–GFP–EB3, His–SNAP–EB3 and His–GFP–PRC1 proteins were purified using a HisTrap HP column and a gradient elution. His–SNAP–EB3, His–SNAP–MCAK$_{1–177}$ and His–SNAP–MCAK$_{584–725}$ were then coupled to SNAP-Cell 647-SiR or SNAP-Cell 546-SiR dyes (S9136S and S9132S, respectively; New England BioLabs) by incubation at 37°C for 30 min or overnight at 4°C. Labelling of His–SNAP–EB3 was around 30% of the total protein, whereas MCAK labelling was around 80–90%, as assessed by following the manufacturer's guidelines. All proteins were further purified using S200 Increase 10/300 gel filtration chromatography (GE Healthcare), in which the columns were pre-equilibrated in gel filtration buffer (25 mM PIPES, pH 6.9, 150 mM NaCl, 300 mM KCl, 5 mM β-mercaptoethanol, 1 mM $MgCl_2$, 1 mM Na-EGTA, and 1 mM ATP). Proteins were frozen in liquid nitrogen within 24 h of cell lysis and stored for up to 3 months at −70°C (Kif18b, MCAK) or 6 months (EB3, PRC1). Protein concentration is reported for its oligomeric state in solution. The activity of frozen proteins was found to be consistent with results from freshly purified proteins within these timescales. Porcine brain tubulin was purified as described (Castoldi and Popov, 2003) and stored in liquid nitrogen long term.

Sample preparation for TIRF microscopy

Samples were prepared as detailed in McHugh et al. (2018). An ATP concentration of 2 mM and a temperature of 30°C were used for all experiments. The stated concentrations of protein (or an equivalent volume of gel filtration buffer, up to a maximum of 3.5% total volume) were added to the final assay buffer {BRB80 buffer (80 mM K-PIPES, 1 mM $MgCl_2$, 1 mM EGTA, pH 6.8) with 2 mM ATP, 0.5 mg/ml casein and an oxygen-scavenging system [0.2 mg/ml glucose oxidase (Sigma-Aldrich, UK), 0.035 mg/ml catalase (C40; Sigma-Aldrich, USA), 4.5 mg/ml glucose (G2133; Sigma-Aldrich, USA) and 140 mM β-mercaptoethanol]}, slides were sealed with Valap [made of equal parts by weight of Vaseline (Unilever, UK and Ireland), Lanolin (NOW Solutions, USA) and uncoloured candle wax] and imaged immediately. For dynamic microtubule experiments, the assay buffer also contained 7–12 µM tubulin (6% Rhodamine-labelled), 1 mg/ml casein and 2 mM GTP. For dynamic microtubule experiments where seeds were double-stabilized with taxol (Sigma-Aldrich, UK) and GMPCPP (NU405S; Jena Biosciences, Germany) (Fig. S5A; Fig. 5D,E), the flow cell was washed with at least ten cell volumes of 1 mg/ml casein (with the exception of data in Fig. 5E, where to provide additional protection against catastrophe, only five cell volumes were used) and then incubated for 5 min before being flowed through with six flow-cell volumes of the assay buffer. Experiments that are compared (in the same graph or table) in this paper were performed in parallel using the same 'master mix' assay buffer with at least three independent repeats, with the exception of data in Fig. S4A–C where two repeats were performed for each condition. For photobleaching analysis, 0.25 nM Kif18b–GFP in BRB80 buffer was introduced to the flow cell and allowed to non-specifically adsorb to the surface. After 3 min, BRB80 with the oxygen-scavenger mix was used to wash away non-adsorbed motors. The sample chamber was imaged using the same conditions as described for single-molecule assays.

TIRF microscopy imaging

Imaging was performed on a Zeiss Axio Observer Z1 TIRF microscope using a 100× NA 1.46 objective and either a Photometrics Evolve Delta

electron-multiplying charge-coupled device camera or a Photometrics Prime 95B sCMOS camera (Teledyne Photometrics, USA) controlled by Zeiss Zen Blue software. For single-molecule experiments in Fig. 1, Fig. S2 and Fig. S3C–E, an Optosplit III beam-splitter (Andor, Oxford Instruments, UK) in bypass mode inserted before the camera provided a further 2× magnification. Depolymerization assays were performed over 10 min at 1 fps or 0.5 fps for two colour imaging; this had no effect on depolymerization rates. Microtubule dynamics assays were performed over 15 min in either one, two or three colours at 0.3 fps. Two-colour imaging of Kif18b–GFP and $SNAP_{546}$–$MCAK_{1–177}$ was performed over 5 min at 0.5 fps. MCAK single-molecule imaging was performed in the GFP channel only at 10 fps (stable microtubules) or 6 fps (dynamic microtubules).

Image analysis

Kymographs were produced using ImageJ (National Institutes of Health), and MCAK single-molecule behaviour, catastrophe length and catastrophe time were manually measured from these kymographs. When analysing microtubule dynamics kymographs, we were unable to consistently detect microtubule growth events that occurred for less than 25 s, so these data were removed from our analysis. Line-scan intensity measurements along microtubules were taken using a fixed threshold in the microtubule fluorescence channel [Rhodamine or HiLyte 647 (TL590M-B and TL670M, respectively; Cytoskeleton, Inc., USA)] to specify the microtubule ends. Intensity measurements for Kif18b motors were taken from kymographs and represent the background-subtracted maximum intensity in the GFP channel along the trajectory of the motor. Graphpad Prism 9 was used for all statistical analysis.

Statistics and reproducibility

Statistical analyses were performed using Prism 9 (GraphPad Software). For the calculation of the error on the median, we report the upper 95% confidence interval (c.i.). No statistical method was used to predetermine sample size. No samples were excluded from the analyses. The investigators were not blinded to allocation during experiments and outcome assessment. All experiments were performed and quantified from at least three independent experiments (unless specified otherwise), and representative data are shown.

Acknowledgements

We thank the Welburn lab and colleagues who took time to read the manuscript. We thank Agata Gluszek for the His–SNAP–EB3 plasmid and providing immunofluorescence images of the Kif18b-knockout cells, and Dave Kelly for Centre Optical Instrumentation Laboratory (COIL) support. The Wellcome Trust Centre for Cell Biology is supported by core funding from the Wellcome Trust (203149). We are grateful to Tarun Kapoor for the His–TEV–GFP–PRC1 plasmid.

Competing interests

The authors declare no competing or financial interests.

Author contributions

Conceptualization: J.P.I.W.; Methodology: T.M.; Validation: J.P.I.W., T.M.; Formal analysis: J.P.I.W., T.M.; Investigation: J.P.I.W., T.M.; Resources: J.P.I.W.; Writing - original draft: J.P.I.W., T.M.; Writing - review & editing: J.P.I.W., T.M.; Visualization: T.M.; Supervision: J.P.I.W.; Project administration: J.P.I.W.; Funding acquisition: J.P.I.W.

Funding

J.P.I.W. is supported by a Wellcome Trust Senior Research Fellowship (207430). J.P.I.W. is also a EMBO Young Investigator. Open Access funding provided by the University of Edinburgh. Deposited in PMC for immediate release.

Peer review history

The peer review history is available online at https://journals.biologists.com/jcs/article-lookup/doi/10.1242/jcs.260144.

References

Belmont, L. D., Hyman, A. A., Sawin, K. E. and Mitchison, T. J. (1990). Real-time visualization of cell cycle-dependent changes in microtubule dynamics in cytoplasmic extracts. *Cell* **62**, 579-589. doi:10.1016/0092-8674(90)90022-7

Buey, R. M., Sen, I., Kortt, O., Mohan, R., Gfeller, D., Veprintsev, D., Kretzschmar, I., Scheuermann, J., Neri, D., Zoete, V. et al. (2012). Sequence determinants of a microtubule tip localization signal (MtLS). *J. Biol. Chem.* **287**, 28227-28242. doi:10.1074/jbc.M112.373928

Cameron, L. A., Yang, G., Cimini, D., Canman, J. C., Kisurina-Evgenieva, O., Khodjakov, A., Danuser, G. and Salmon, E. D. (2006). Kinesin 5-independent poleward flux of kinetochore microtubules in PtK1 cells. *J. Cell Biol.* **173**, 173-179. doi:10.1083/jcb.200601075

Castoldi, M. and Popov, A. V. (2003). Purification of brain tubulin through two cycles of polymerization-depolymerization in a high-molarity buffer. *Protein Expr. Purif.* **32**, 83-88. doi:10.1016/S1046-5928(03)00218-3

Cooper, J. R., Wagenbach, M., Asbury, C. L. and Wordeman, L. (2010). Catalysis of the microtubule on-rate is the major parameter regulating the depolymerase activity of MCAK. *Nat. Struct. Mol. Biol.* **17**, 77-82. doi:10.1038/nsmb.1728

Cottingham, F. R. and Hoyt, M. A. (1997). Mitotic spindle positioning in Saccharomyces cerevisiae is accomplished by antagonistically acting microtubule motor proteins. *J. Cell Biol.* **138**, 1041-1053. doi:10.1083/jcb.138.5.1041

Domnitz, S. B., Wagenbach, M., Decarreau, J. and Wordeman, L. (2012). MCAK activity at microtubule tips regulates spindle microtubule length to promote robust kinetochore attachment. *J. Cell Biol.* **197**, 231-237. doi:10.1083/jcb.201108147

Ems-McClung, S. C. and Walczak, C. E. (2010). Kinesin-13s in mitosis: Key players in the spatial and temporal organization of spindle microtubules. *Semin. Cell Dev. Biol.* **21**, 276-282. doi:10.1016/j.semcdb.2010.01.016

Ems-McClung, S. C., Hainline, S. G., Devare, J., Zong, H., Cai, S., Carnes, S. K., Shaw, S. L. and Walczak, C. E. (2013). Aurora B Inhibits MCAK Activity through a Phosphoconformational Switch that Reduces Microtubule Association. *Curr. Biol.* **23**, 2491-2499. doi:10.1016/j.cub.2013.10.054

Friel, C. T. and Welburn, J. P. (2018). Parts list for a microtubule depolymerising kinesin. *Biochem. Soc. Trans.* **46**, 1665-1672. doi:10.1042/BST20180350

Gardner, M. K., Zanic, M., Gell, C., Bormuth, V. and Howard, J. (2011). Depolymerizing kinesins Kip3 and MCAK shape cellular microtubule architecture by differential control of catastrophe. *Cell.* **147**, 1092-1103. doi:10.1016/j.cell.2011.10.037

Goshima, G., Wollman, R., Stuurman, N., Scholey, J. M. and Vale, R. D. (2005). Length control of the metaphase spindle. *Curr. Biol.* **15**, 1979-1988. doi:10.1016/j.cub.2005.09.054

Gupta, M. L., Jr, Carvalho, P., Roof, D. M. and Pellman, D. (2006). Plus end-specific depolymerase activity of Kip3, a kinesin-8 protein, explains its role in positioning the yeast mitotic spindle. *Nat. Cell Biol.* **8**, 913-923. doi:10.1038/ncb1457

Helenius, J., Brouhard, G., Kalaidzidis, Y., Diez, S. and Howard, J. (2006). The depolymerizing kinesin MCAK uses lattice diffusion to rapidly target microtubule ends. *Nature* **441**, 115-119. doi:10.1038/nature04736

Honnappa, S., Gouveia, S. M., Weisbrich, A., Damberger, F. F., Bhavesh, N. S., Jawhari, H., Grigoriev, I., van Rijssel, F. J., Buey, R. M., Lawera, A. et al. (2009). An EB1-binding motif acts as a microtubule tip localization signal. *Cell* **138**, 366-376. doi:10.1016/j.cell.2009.04.065

Huang, H., Feng, J., Famulski, J., Rattner, J. B., Liu, S. T., Kao, G. D., Muschel, R., Chan, G. K. and Yen, T. J. (2007). Tripin/hSgo2 recruits MCAK to the inner centromere to correct defective kinetochore attachments. *J. Cell Biol.* **177**, 413-424. doi:10.1083/jcb.200701122

Jumper, J., Evans, R., Pritzel, A., Green, T., Figurnov, M., Ronneberger, O., Tunyasuvunakool, K., Bates, R., Zidek, A., Potapenko, A. et al. (2021). Highly accurate protein structure prediction with AlphaFold. *Nature* **596**, 583-589. doi:10.1038/s41586-021-03819-2

Lee, Y. M., Kim, E., Park, M., Moon, E., Ahn, S. M., Kim, W., Hwang, K. B., Kim, Y. K., Choi, W. and Kim, W. (2010). Cell cycle-regulated expression and subcellular localization of a kinesin-8 member human KIF18B. *Gene* **466**, 16-25. doi:10.1016/j.gene.2010.06.007

Maney, T., Hunter, A. W., Wagenbach, M. and Wordeman, L. (1998). Mitotic centromere-associated kinesin is important for anaphase chromosome segregation. *J. Cell Biol.* **142**, 787-801. doi:10.1083/jcb.142.3.787

Maney, T., Wagenbach, M. and Wordeman, L. (2001). Molecular dissection of the microtubule depolymerizing activity of mitotic centromere-associated kinesin. *J. Biol. Chem.* **276**, 34753-34758. doi:10.1074/jbc.M106626200

Maurer, S. P., Bieling, P., Cope, J., Hoenger, A. and Surrey, T. (2011). GTPgammaS microtubules mimic the growing microtubule end structure recognized by end-binding proteins (EBs). *Proc. Natl. Acad. Sci. USA* **108**, 3988-3993. doi:10.1073/pnas.1014758108

Maurer, S. P., Cade, N. I., Bohner, G., Gustafsson, N., Boutant, E. and Surrey, T. (2014). EB1 accelerates two conformational transitions important for microtubule maturation and dynamics. *Curr. Biol.* **24**, 372-384. doi:10.1016/j.cub.2013.12.042

McHugh, T., Gluszek, A. A. and Welburn, J. P. I. (2018). Microtubule end tethering of a processive kinesin-8 motor Kif18b is required for spindle positioning. *J. Cell Biol.* **217**, 2403-2416. doi:10.1083/jcb.201705209

McHugh, T., Zou, J., Volkov, V. A., Bertin, A., Talapatra, S. K., Rappsilber, J., Dogterom, M. and Welburn, J. P. I. (2019). The depolymerase activity of MCAK shows a graded response to Aurora B kinase phosphorylation through allosteric regulation. *J. Cell Sci.* **132**, jcs228353. doi:10.1242/jcs.228353

McIntosh, J. R., O'Toole, E., Morgan, G., Austin, J., Ulyanov, E., Ataullakhanov, F. and Gudimchuk, N. (2018). Microtubules grow by the addition of bent guanosine triphosphate tubulin to the tips of curved protofilaments. *J. Cell Biol.* **217**, 2691-2708. doi:10.1083/jcb.201802138

Miller, R. K., Heller, K. K., Frisen, L., Wallack, D. L., Loayza, D., Gammie, A. E. and Rose, M. D. (1998). The kinesin-related proteins, Kip2p and Kip3p, function differently in nuclear migration in yeast. *Mol. Biol. Cell* **9**, 2051-2068. doi:10.1091/mbc.9.8.2051

Mirdita, M., Schütze, K., Moriwaki, Y., Heo, L., Ovchinnikov, S. and Steinegger, M. (2022). ColabFold - Making protein folding accessible to all. *bioRxiv*. doi:10.1101/2021.08.15.456425.

Mitchison, T. and Kirschner, M. (1984). Dynamic instability of microtubule growth. *Nature* **312**, 237-242. doi:10.1038/312237a0

Montenegro Gouveia, S., Leslie, K., Kapitein, L. C., Buey, R. M., Grigoriev, I., Wagenbach, M., Smal, I., Meijering, E., Hoogenraad, C. C., Wordeman, L. et al. (2010). In vitro reconstitution of the functional interplay between MCAK and EB3 at microtubule plus ends. *Curr. Biol.* **20**, 1717-1722. doi:10.1016/j.cub.2010.08.020

Moore, A. T., Rankin, K. E., von Dassow, G., Peris, L., Wagenbach, M., Ovechkina, Y., Andrieux, A., Job, D. and Wordeman, L. (2005). MCAK associates with the tips of polymerizing microtubules. *J. Cell Biol.* **169**, 391-397. doi:10.1083/jcb.200411089

Piehl, M. and Cassimeris, L. (2003). Organization and dynamics of growing microtubule plus ends during early mitosis. *Mol. Biol. Cell* **14**, 916-925. doi:10.1091/mbc.e02-09-0607

Rankin, K. E. and Wordeman, L. (2010). Long astral microtubules uncouple mitotic spindles from the cytokinetic furrow. *J. Cell Biol.* **190**, 35-43. doi:10.1083/jcb.201004017

Rischitor, P. E., Konzack, S. and Fischer, R. (2004). The Kip3-like kinesin KipB moves along microtubules and determines spindle position during synchronized mitoses in Aspergillus nidulans hyphae. *Eukaryot. Cell* **3**, 632-645. doi:10.1128/EC.3.3.632-645.2004

Roth, D., Fitton, B. P., Chmel, N. P., Wasiluk, N. and Straube, A. (2018). Spatial positioning of EB family proteins at microtubule tips involves distinct nucleotide-dependent binding properties. *J. Cell Sci.* **132**, jcs219550. doi:10.1242/jcs.219550

Savoian, M. S. and Glover, D. M. (2010). Drosophila Klp67A binds prophase kinetochores to subsequently regulate congression and spindle length. *J. Cell Sci.* **123**, 767-776. doi:10.1242/jcs.055905

Shin, Y., Du, Y., Collier, S. E., Ohi, M. D., Lang, M. J. and Ohi, R. (2015). Biased Brownian motion as a mechanism to facilitate nanometer-scale exploration of the microtubule plus end by a kinesin-8. *Proc. Natl. Acad. Sci. USA* **112**, E3826-E3835.

Shrestha, S., Hazelbaker, M., Yount, A. L. and Walczak, C. E. (2018). Emerging insights into the function of kinesin-8 proteins in microtubule length regulation. *Biomolecules* **9**, 1. doi:10.3390/biom9010001

Sironi, L., Solon, J., Conrad, C., Mayer, T. U., Brunner, D. and Ellenberg, J. (2011). Automatic quantification of microtubule dynamics enables RNAi-screening of new mitotic spindle regulators. *Cytoskeleton (Hoboken)* **68**, 266-278. doi:10.1002/cm.20510

Stout, J. R., Yount, A. L., Powers, J. A., Leblanc, C., Ems-McClung, S. C. and Walczak, C. E. (2011). Kif18B interacts with EB1 and controls astral microtubule length during mitosis. *Mol. Biol. Cell* **22**, 3070-3080. doi:10.1091/mbc.e11-04-0363

Stumpff, J., Du, Y., English, C. A., Maliga, Z., Wagenbach, M., Asbury, C. L., Wordeman, L. and Ohi, R. (2011). A Tethering Mechanism Controls the Processivity and Kinetochore-Microtubule Plus-End Enrichment of the Kinesin-8 Kif18A. *Mol. Cell* **43**, 764-775. doi:10.1016/j.molcel.2011.07.022

Su, X., Qiu, W., Gupta, M. L., Jr, Pereira-Leal, J. B., Reck-Peterson, S. L. and Pellman, D. (2011). Mechanisms underlying the dual-mode regulation of microtubule dynamics by kip3/kinesin-8. *Mol. Cell* **43**, 751-763. doi:10.1016/j.molcel.2011.06.027

Su, X., Arellano-Santoyo, H., Portran, D., Gaillard, J., Vantard, M., Thery, M. and Pellman, D. (2013). Microtubule-sliding activity of a kinesin-8 promotes spindle assembly and spindle-length control. *Nat. Cell Biol.* **15**, 948-957. doi:10.1038/ncb2801

Subramanian, R., Wilson-Kubalek, E. M., Arthur, C. P., Bick, M. J., Campbell, E. A., Darst, S. A., Milligan, R. A. and Kapoor, T. M. (2010). Insights into antiparallel microtubule crosslinking by PRC1, a conserved nonmotor microtubule binding protein. *Cell* **142**, 433-443. doi:10.1016/j.cell.2010.07.012

Talapatra, S. K., Harker, B. and Welburn, J. P. (2015). The C-terminal region of the motor protein MCAK controls its structure and activity through a conformational switch. *Elife* **4**, e06421. doi:10.7554/eLife.06421

Tanenbaum, M. E., Macurek, L., Janssen, A., Geers, E. F., Alvarez-Fernandez, M. and Medema, R. H. (2009). Kif15 cooperates with eg5 to promote bipolar spindle assembly. *Curr. Biol.* **19**, 1703-1711. doi:10.1016/j.cub.2009.08.027

Tanenbaum, M. E., Macurek, L., van der Vaart, B., Galli, M., Akhmanova, A. and Medema, R. H. (2011). A Complex of Kif18b and MCAK Promotes Microtubule Depolymerization and Is Negatively Regulated by Aurora Kinases. *Curr. Biol.* **21**, 1356-1365. doi:10.1016/j.cub.2011.07.017

Tanenbaum, M. E., Gilbert, L. A., Qi, L. S., Weissman, J. S. and Vale, R. D. (2014). A protein-tagging system for signal amplification in gene expression and fluorescence imaging. *Cell* **159**, 635-646. doi:10.1016/j.cell.2014.09.039

van Heesbeen, R. G., Raaijmakers, J. A., Tanenbaum, M. E., Halim, V. A., Lelieveld, D., Lieftink, C., Heck, A. J., Egan, D. A. and Medema, R. H. (2016). Aurora A, MCAK, and Kif18b promote Eg5-independent spindle formation. *Chromosoma* **126**, 473-486. doi:10.1007/s00412-016-0607-4

Walczak, C. E., Mitchison, T. J. and Desai, A. (1996). XKCM1: a Xenopus kinesin-related protein that regulates microtubule dynamics during mitotic spindle assembly. *Cell* **84**, 37-47. doi:10.1016/S0092-8674(00)80991-5

Walczak, C. E., Gayek, S. and Ohi, R. (2013). Microtubule-depolymerizing kinesins. *Annu. Rev. Cell Dev. Biol.* **29**, 417-441. doi:10.1146/annurev-cellbio-101512-122345

Walczak, C. E., Zong, H., Jain, S. and Stout, J. R. (2016). Spatial regulation of astral microtubule dynamics by Kif18B in PtK cells. *Mol. Biol. Cell* **27**, 3021-3030. doi:10.1091/mbc.e16-04-0254

Welburn, J. P. and Cheeseman, I. M. (2012). The microtubule-binding protein Cep170 promotes the targeting of the kinesin-13 depolymerase Kif2b to the mitotic spindle. *Mol. Biol. Cell* **23**, 4786-4795. doi:10.1091/mbc.e12-03-0214

Wordeman, L., Wagenbach, M. and Maney, T. (1999). Mutations in the ATP-binding domain affect the subcellular distribution of mitotic centromere-associated kinesin (MCAK). *Cell Biol. Int.* **23**, 275-286. doi:10.1006/cbir.1999.0359

Zong, H., Carnes, S. K., Moe, C., Walczak, C. E. and Ems-McClung, S. C. (2016). The far C-terminus of MCAK regulates its conformation and spindle pole focusing. *Mol. Biol. Cell* **27**, 1451-1464. doi:10.1091/mbc.E15-10-0699

Supplementary Figure 1

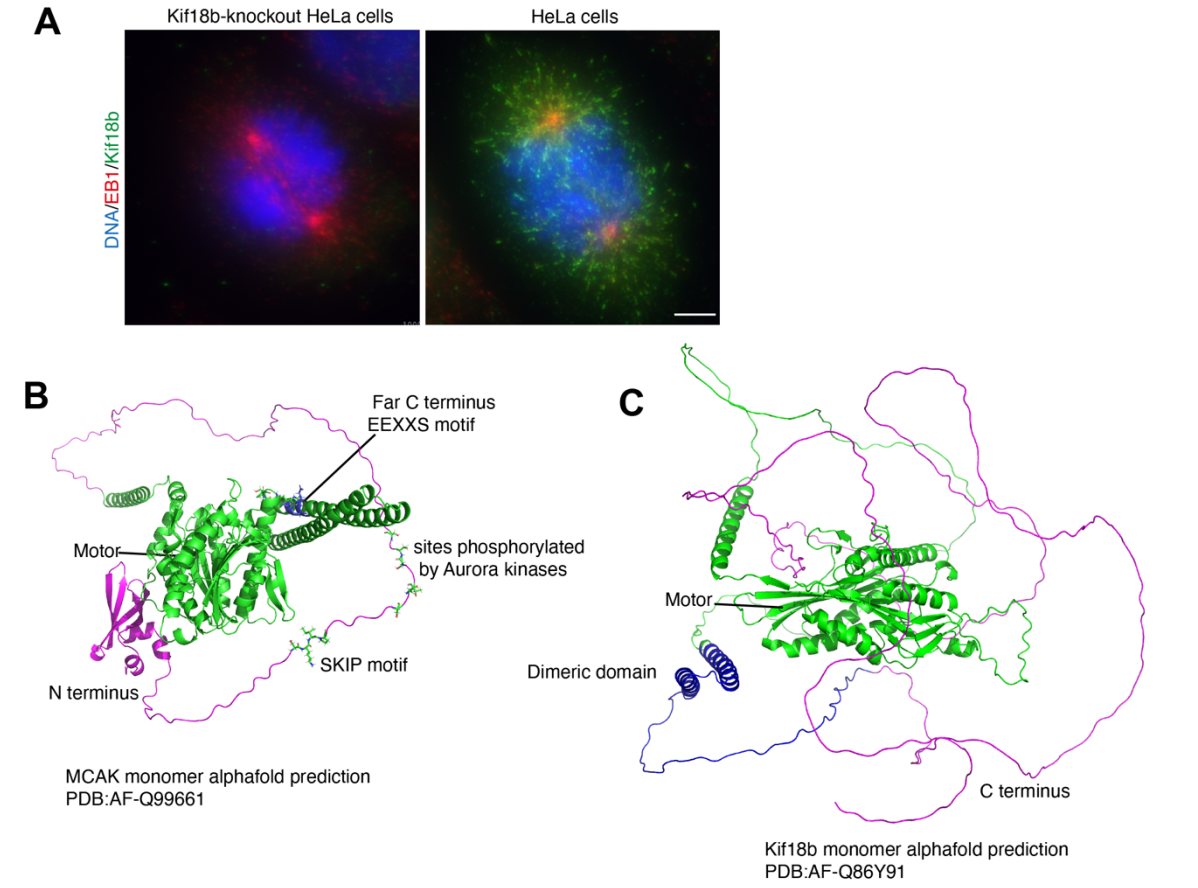

Fig. S1. Structures and purification of proteins used in this study.

A) Representative immunofluorescence images of control Hela cells and Kif18b-knockout HeLa cells stained for DNA, EB1 and Kif18b. Scalebar, 5 μm. B and C) Alphafold2 predicted models of monomeric MCAK and Kif18b drawn as cartoon models. B) Model of MCAK (PDB:AF-Q99661), the N terminus 1-190 is coloured magenta, with the EB binding motif SKIP and the residues phosphorylated by Aurora kinases drawn as stick and balls according to elements. The neck linker, motor and C

terminus are represented in green. The amino acids in the far C terminus essential for intramolecular interactions between the C terminus and the motor (Talapatra et al, 2015, Zong et al, 2016) are shown in blue stick and ball mode. C) Model of Kif18b (PDB:AF-Q86Y91), the N terminus is at the start of the motor domain in green, a dimeric domain (McHugh et al, 2018) is painted blue and the tail containing the EB binding region is of low complexity and represented in magenta. D) Coomassie stained gel of purified proteins used in the experiments in this paper. E) Coomassie stained gel showing Kif18b-GFP-His bound to Ni^{2+} beads after incubation and washing with SNAP-MCAK$_{1-177}$ and SNAP-MCAK$_{178-725}$.

Supplementary Figure 2

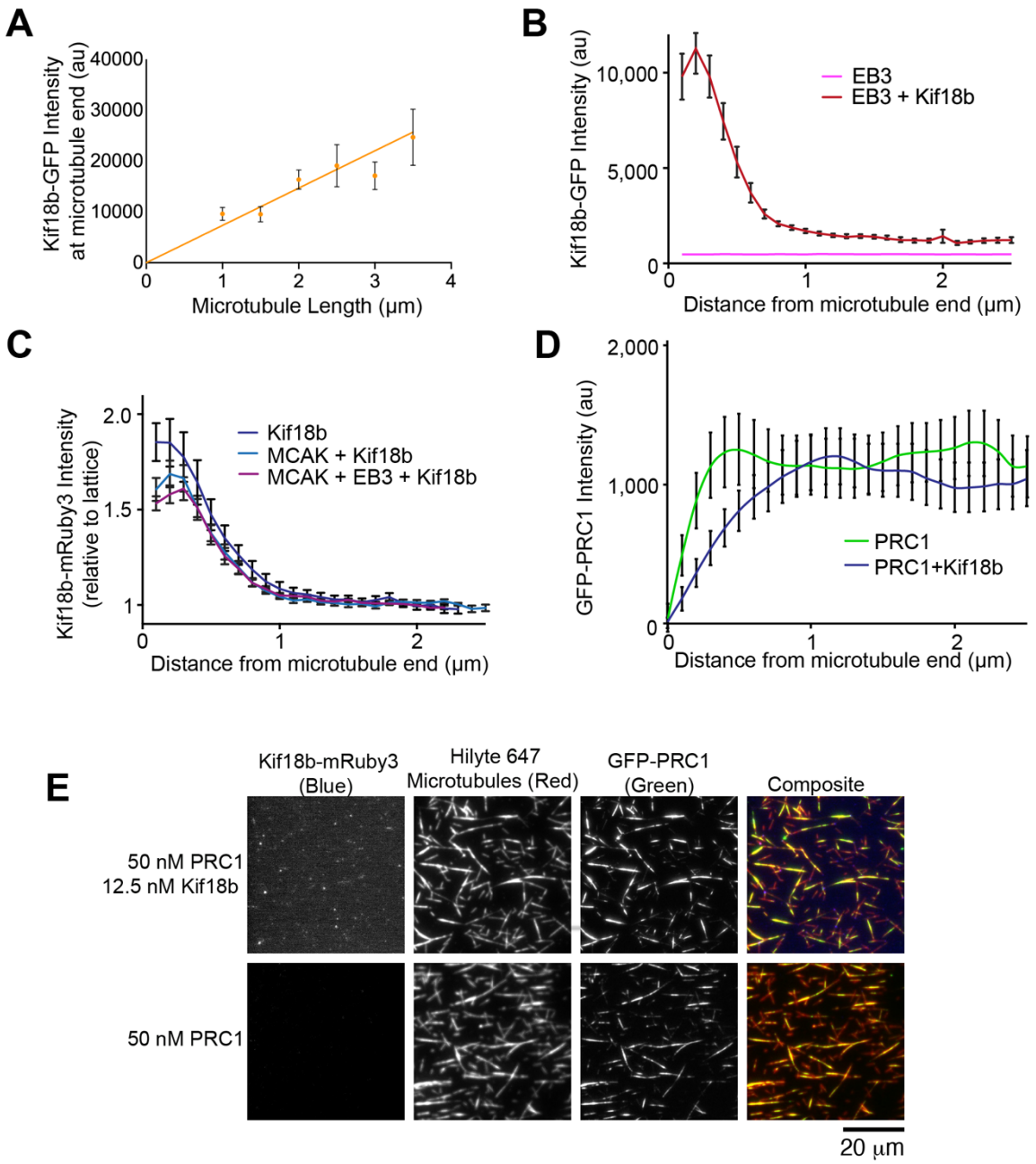

Fig. S2. Kif18b accumulates at microtubule plus ends but does not enrich the microtubule-associated protein PRC1 there. A) Dependence of maximum fluorescence intensity of Kif18b-GFP at microtubule plus ends on the length of microtubule, 0.5 μm bins, mean and S.E. n=42, Kif18b-GFP intensity showed a positive correlation with microtubule length. P-value<0.0001. B) Quantification of the GFP fluorescence intensity along the microtubule in the presence of 50 nM SNAP647-EB3 and 12.5 nM (red, n = 41) or 0 nM (pink, n = 44)

of Kif18b-GFP (mean and S.E). C) Quantification of mRuby3 fluorescence intensity (mean and S.E) along the microtubule in the presence of 12.5 nM Kif18b-mRuby3 alone (dark blue, n = 64), with 12.5 nM MCAK-GFP (blue, n = 90), with 12.5 nM MCAK-GFP and 50 nM SNAP647-EB3 (purple, n = 116). Kolmogorov-Smirnov test at 0.2 µm, Kif18b vs Kif18b + MCAK, ns (P=0.1279), Kif18b vs Kif18b + MCAK + EB3, **** P<0.0001. D) Quantification of GFP fluorescence intensity along the microtubule in the presence of 50 nM GFP-PRC1 and 25 nM (dark blue, n = 26) or 0 nM (green, n = 26) of Kif18b-mRuby3 (mean and S.D). E) Representative images of Kif18b-mRuby3 (blue), GFP-PRC1 (green) localization on taxol- and GMPCPP-stabilized microtubules (HiLyte647- tubulin, red). Scale Bar 20 µm.

Supplementary Figure 3

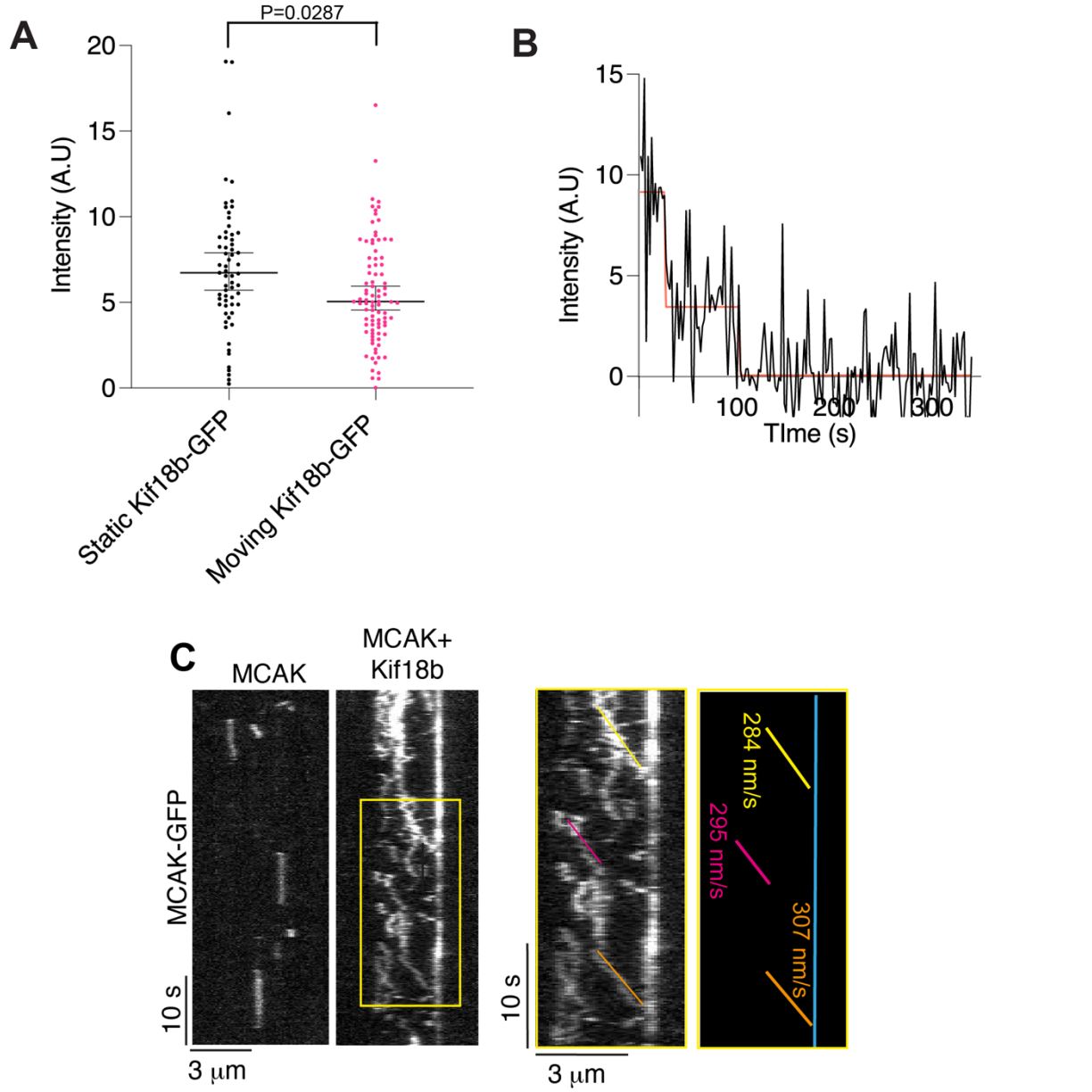

Fig. S3. Properties of MCAK on microtubules in the presence of Kif18b. A) Fluorescence intensity measurements median and 95% C.I. Kif18b-GFP on microtubules for static and processive Kif18b (n= 65 and 97 respectively). Asterisks indicate Kolmogorov-Smirnov significance *, P=0.0287. B) Corresponding intensity profile for a motor in a. Horizontal red lines show the mean intensity for the respective sections of the profile. C) Example kymographs for 0.25 nM MCAK-GFP and 4.75 nM unlabeled MCAK showing the increase in diffusive behavior in the presence of Kif18b-mRuby3. Scale bars, 10 seconds (vertical) and 3 μm (horizontal). Highlighted section shows tracks where MCAK moves directionally towards one end of the microtubule. D) Mean squared displacement plotted against the time over which it was measured for 0.25 nM MCAK-GFP motors in the presence of 4.75 nM unlabeled MCAK and 0 nM (green, n = 246) or 10 nM Kif18b-mRuby3 (blue, n = 820), mean and S.E. Fitted with a linear curve from which the diffusion coefficient D can be measured ($2Dt = \langle x^2 \rangle$). E) Frequencies of microtubule residency time for MCAK-GFP motors on GMPCPP stable microtubules with 0 nM (green, n=247) and 10 nM (blue, n = 820) Kif18b-mRuby3, mean and S.E. are fitted with exponential curves to give mean residency times $t_{1/2}$.

Supplementary figure 4

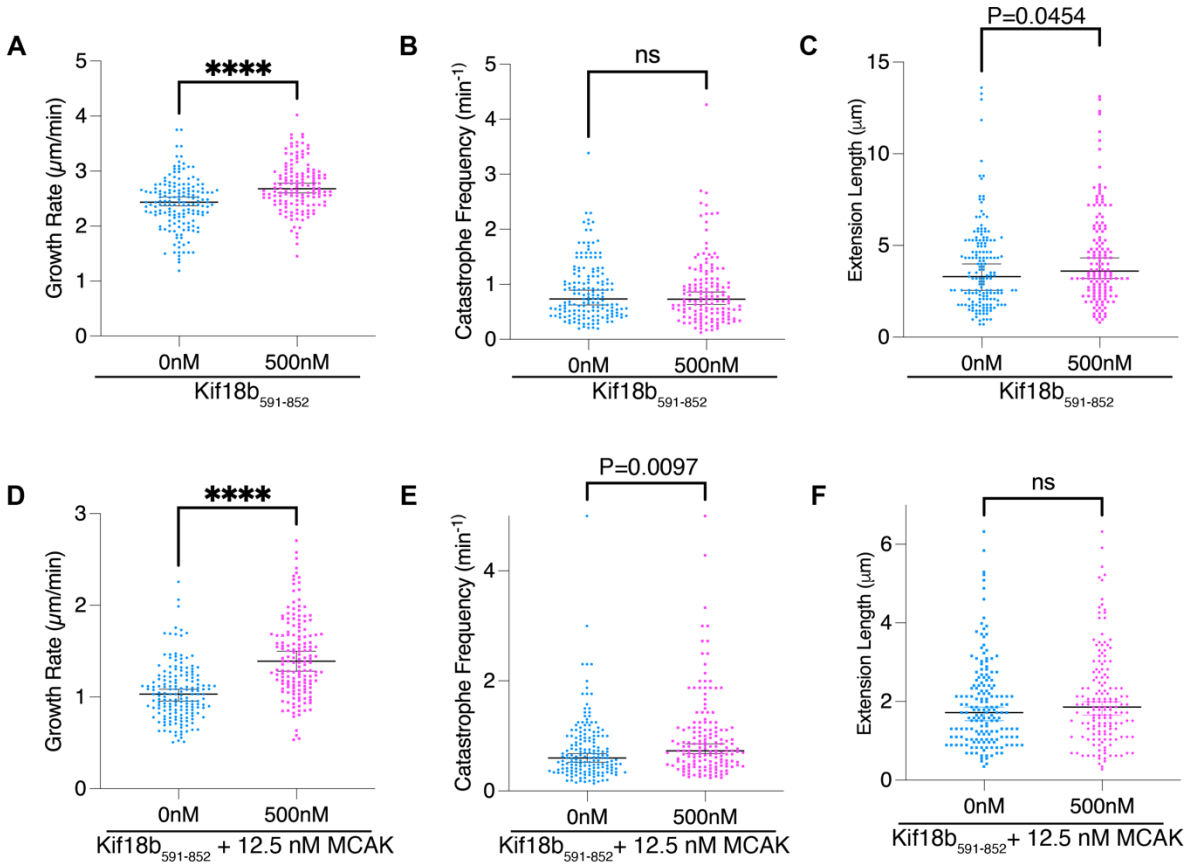

Fig. S4. The C-terminus of Kif18b increases the growth rate of dynamic microtubules. A) Measured growth rates of dynamic microtubule extensions in the absence and presence of Kif18b591-852. B) Microtubule catastrophe frequency and C) length of dynamic microtubule extensions in the absence and presence of 500 nM Kif18b591-852. For each condition, n=188 and 175 respectively, from 2 independent repeats. D) Measured growth rates of dynamic microtubule extensions in the absence and presence of increasing concentration of Kif18b591-852. E) Microtubule catastrophe frequency and F) length of dynamic microtubule extensions in the presence of 12.5 nM MCAK and with and without 500 nM Kif18b591-852. For each condition, n=188 and 175 respectively, from 2 independent repeats. Kolmogorov-Smirnov test, P-value, **** P<0.0001, ** P=0.0097 for catastrophe frequency (E) and * P=0.0454 for microtubule length (C). Median and 95% C.I are presented.

Supplementary Figure 5

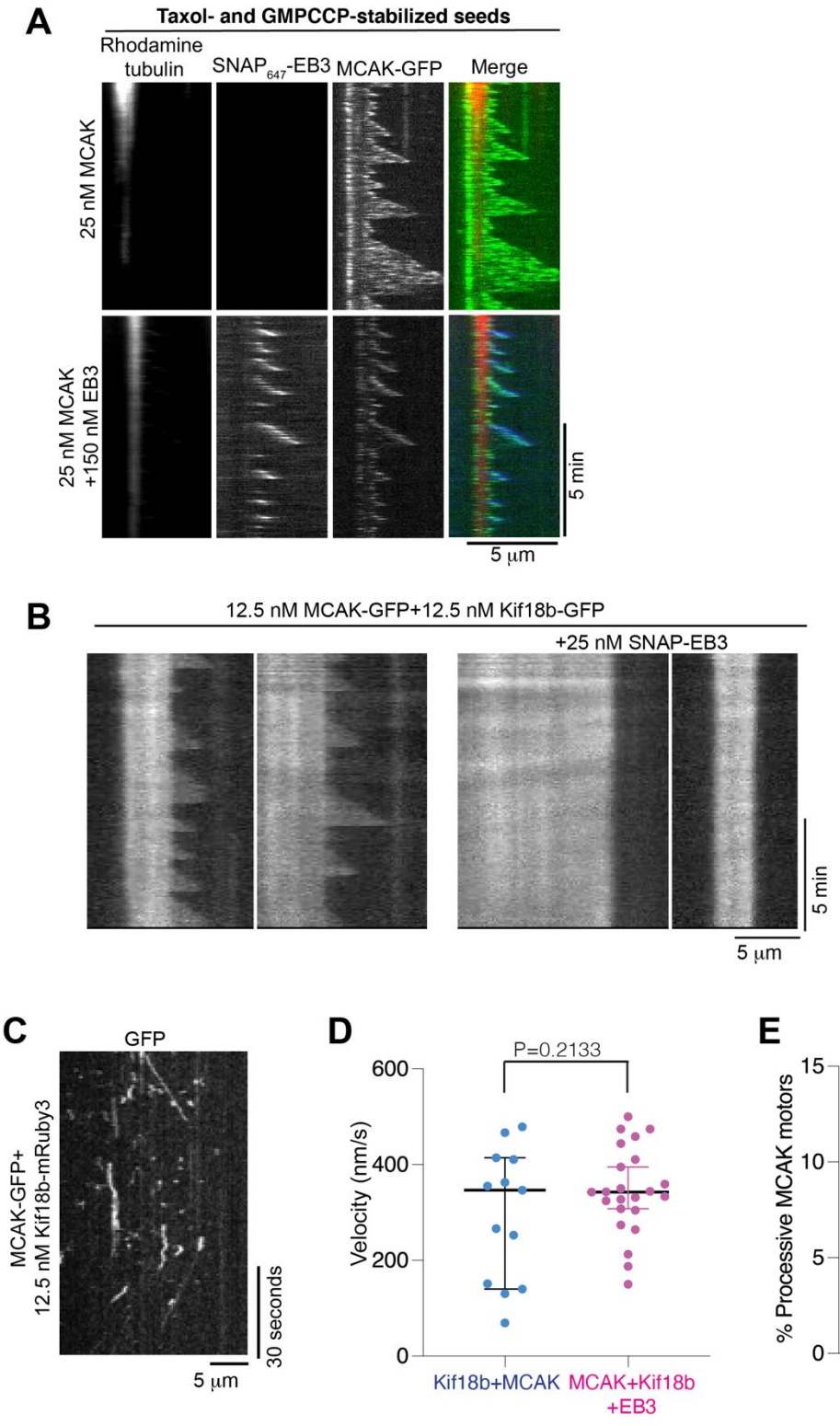

Fig. S5. MCAK directional movement and plus-end accumulation is driven by Kif18b and EB3. A) Representative kymographs of dynamic microtubules with 12 µM rhodamine tubulin, and 25 nM MCAK-GFP with or without 150 nM SNAP647-EB3. Scale 5 mins (vertical) and 5 µm (horizontal). Seeds are taxol and GMPCCP stabilized. B) Representative kymographs of dynamic microtubules in the presence of 12.5 nM

Kif18b-GFP and 12.5 nM MCAK-GFP with or without 25nM SNAP-EB3 with 12 μM tubulin. Scale 5 mins (vertical) and 5 μm (horizontal). C) Example kymograph for 5nM MCAK-GFP in the presence of 12.5nM Kif18b-mRuby3 on dynamic microtubule lattice showing both diffusive and processive behaviours. Scale bars, 30 seconds (vertical) and 5 μm (horizontal). D) Velocities of processive tracks of with 5 nM MCAK-GFP and 12.5 nM Kif18b-mRuby alone and with 25 nM $SNAP_{647}$-EB3 (n =13 and n=23 respectively). T-test, P-value, ns P= 0.2133. E) Percentage of MCAK-GFP microtubule binding events lasting over 10 frames (1.6 seconds) that show processive behaviour with 5 nM MCAK-GFP, 12.5 nM Kif18b-mRuby alone and with 25 nM $SNAP_{647}$-EB3 (n=286 and 251 respectively). Two tailed Binomial Test, P-value, ** P = 0.002.

Table S1. Summary of depolymerization rates, median and 95% C.I. and n values for the data shown in Figure 3D.

25 nM dimeric motor	Depolymerization Rate (μm/min) Median ± 95% C.I.	N
Control	0.015±0.006	110
$Kif18b_{FL}$	0.000±0.000	74
$Kif18b_{1-590}$	0.027±0.003	272
MCAK	0.390±0.092	82
$Kif18b_{1-590}$ + MCAK	0.440±0.060	104
$Kif18b_{FL}$ + MCAK (+ end)	0.036±0.031	49
$Kif18b_{FL}$ + MCAK (- end)	0.412±0.152	49

Table S2. Summary of depolymerization rates, median and 95% C.I. and n values for the data shown in Figure 3E.

	Depolymerization Rate (μm/min) Median±95% C.I.	N
Control	0.052±0.013	94
25nM MCAK	0.304±0.067	113
500 nM $Kif18b_{591-852}$ + 25nM MCAK	0.105±0.016	165
250 nM $Kif18b_{1-590}$ + 25nM MCAK	1.534±0.100	127

Table S3. Summary of landing rates, median and 95% C.I. and n values for the data shown in Figure 3F.

	Landing Rate (μm^{-1} s^{-1}) Median±95% C.I.	N
MCAK	0.0168±0.0044	53
Kif18b$_{591-852}$ + MCAK	0.0177±0.0024	59

Table S4. Summary of catastrophe frequency and microtubule length (median and 95% C.I. and n values) for figure 4A-C. A tubulin concentration of 12 μM was used.

	Catastrophe Frequency		Microtubule Length	
	Median (/min) and upper 95% CI	**N**	**Median (μm) and upper 95% CI**	**N**
0 nM MCAK	0.34±0.04	184	3.85±0.69	184
12.5 nM MCAK	0.51±0.07	350	2.68±0.21	350
25 nM MCAK	1.1±0.2	297	1.51±0.14	297

Table S5. Summary of catastrophe frequency and microtubule length for figure 4D-F. A tubulin concentration of 7 μM was used (median and 95% C.I. and n values).

	Catastrophe Frequency		Catastrophe Length	
	Median (/min) and upper 95% CI	**N**	**Median (μm) and upper 95% CI**	**N**
12.5 nM MCAK	1.02±0.12	283	1.87±0.19	306
25 nM EB3	0.94±0.07	178	2.84±0.36	182
12.5 nM MCAK + 50 nM EB3	1.16±0.07	346	1.71±0.11	395

Table S6. Summary of catastrophe frequency and microtubule length for figure 4G-I. A tubulin concentration of 7 μM was used. (median and 95% C.I. and n values).

	Catastrophe Frequency		Catastrophe Length	
	Median (/min) and upper 95% CI	**N**	**Median (μm) and upper 95% CI**	**N**
12.5 nM MCAK	0.88±0.14	108	2.11±0.35	124
12.5 nM Kif18b	0.79±0.07	597	2.64±0.20	608
12.5 nM MCAK + 12.5 nM Kif18b	1.19±0.09	152	1.60±0.24	187

Table S7. Summary of catastrophe frequency and microtubule length in the presence of MCAK, Kif18b and EB3. A tubulin concentration of 12 μM was used. (median and 95% C.I. and n values).

	Catastrophe Frequency		Microtubule Length	
	Median (/min) and upper 95% CI	**N**	**Median (μm) and upper 95% CI**	**N**
5 nM MCAK + 25nM EB3	0.34±0.08	70	3.00±1.13	70
12.5nM Kif18b +25nM EB3	0.52±0.09	98	2.51±0.72	98
5 nM MCAK + 12.5nM Kif18b	0.43±0.14	63	1.56±1.1	63
5 nM MCAK + 12.5nM Kif18b +25nM EB3	0.74±0.12	105	1.63±0.398	105

Table S8. Summary of the constructs and cloning details used in this study.

Insect cell expression	**Vector**
Kif18b-mRuby3-His	pFL-mRuby3-His
pFL-mRuby3-His	pFL
Bacterial expression	
Kif18b$_{591-852}$-6xHis	pET3aTr
His-TEV-SNAP-MCAK$_{1-177}$	pAG17
His-TEV-SNAP-MCAK$_{584-725}$	pAG17
His-TEV-SNAP-MCAK$_{178-725}$	pAG17
His-TEV-SNAP-EB3	pAG17
His-GFP-EB3	pAG17
pAG17	pST50Tr-HISNDHFR one NdeI site removed

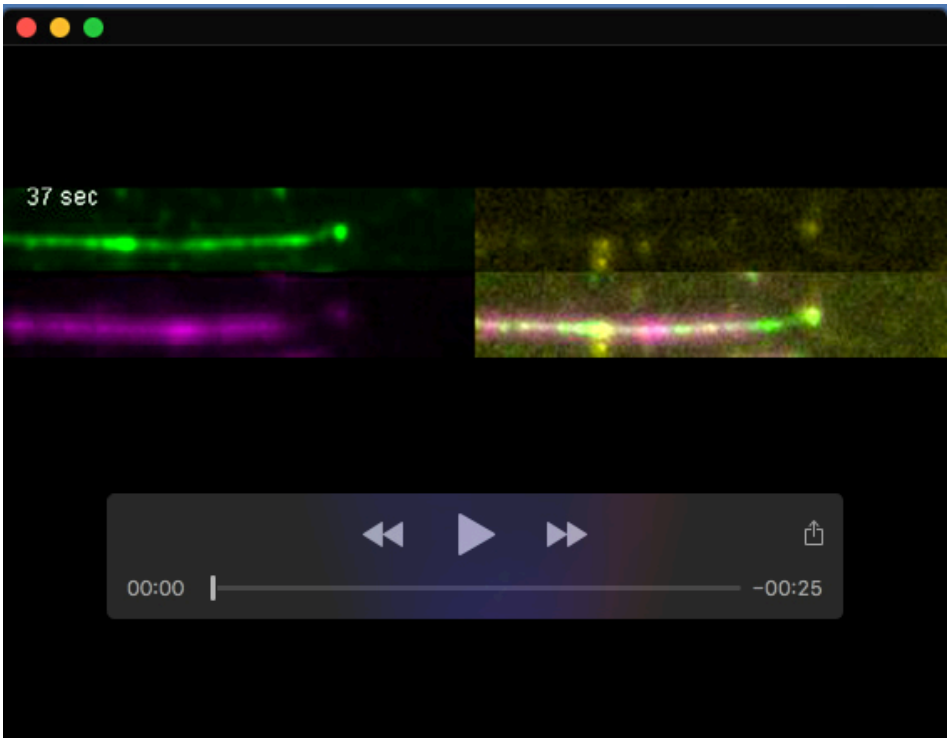

Movie 1. Kif18b moves MCAK and EB3 to the plus ends of growing microtubules

Dynamic microtubules in the presence of 25 nM MCAK-GFP (green), 25 nM Kif18b-mRuby3 (red), 100 nM SNAP$_{647}$-EB3 (blue) with 12 μM tubulin. Seeds were stabilized with taxol and GMPCPP.

Journal of Cell Science • Supplementary information